Available online at www.sciencedirect.com
ScienceDirect
Journal of Computational Physics 226 (2007) 104–130
JOURNAL OF COMPUTATIONAL PHYSICS
www.elsevier.com/locate/jcp

Computing wave functions of nonlinear Schrödinger equations: A time-independent approach

S.-L. Chang [a], C.-S. Chien [b,*], B.-W. Jeng [c]

[a] *Center for General Education, Southern Taiwan University of Technology, Tainan 710, Taiwan*
[b] *Department of Applied Mathematics, National Chung Hsing University, 250, Kuo Kuang Road, Taichung 402, Taiwan*
[c] *Department of Applied Mathematics, National Chiao Tung University, Hsinchu 300, Taiwan*

Received 4 July 2006; received in revised form 9 February 2007; accepted 28 March 2007
Available online 11 April 2007

Abstract

We present a novel algorithm for computing the ground-state and excited-state solutions of M-coupled nonlinear Schrödinger equations (MCNLS). First we transform the MCNLS to the stationary state ones by using separation of variables. The energy level of a quantum particle governed by the Schrödinger eigenvalue problem (SEP) is used as an initial guess to computing their counterpart of a nonlinear Schrödinger equation (NLS). We discretize the system via centered difference approximations. A predictor–corrector continuation method is exploited as an iterative method to trace solution curves and surfaces of the MCNLS, where the chemical potentials are treated as continuation parameters. The wave functions can be easily obtained whenever the solution manifolds are numerically traced. The proposed algorithm has the advantage that it is unnecessary to discretize or integrate the partial derivatives of wave functions. Moreover, the wave functions can be computed for any time scale. Numerical results on the ground-state and excited-state solutions are reported, where the physical properties of the system such as isotropic and nonisotropic trapping potentials, mass conservation constraints, and strong and weak repulsive interactions are considered in our numerical experiments.

Keywords: Bose–Einstein condensates; Gross–Pitaevskii equation; Wave functions; Liapunov–Schmidt reduction; Continuation; Centered difference method; Disk

1. Introduction

In this paper we are concerned with wave functions of M-coupled nonlinear Schrödinger equations (MCNLS), also known as the Gross–Pitaevskii equations (GPE) [35]

* Corresponding author. Tel./fax: +886 4 22873028.
E-mail address: cschien@amath.nchu.edu.tw (C.-S. Chien).

0021-9991/$ - see front matter
doi:10.1016/j.jcp.2007.03.028

$$\begin{aligned} &\mathrm{i}\frac{\partial}{\partial t}\Phi_j = -\Delta\Phi_j + V_j(x)\Phi_j + \mu_j|\Phi_j|^2\Phi_j + \sum_{i\neq j}\beta_{ij}|\Phi_i|^2\Phi_j \quad \text{for } x\in\mathbf{R}^2,\ t>0,\\ &\Phi_j = \Phi_j(x,t)\in\mathbf{C}, \quad j=1,\ldots,M,\\ &\Phi_j(x,t)\to 0 \quad \text{as } |x|\to+\infty,\ t>0. \end{aligned} \tag{1}$$

Here the solutions Φ_j represent the jth component of the beam in Kerr-like photorefractive media [6], $V_j(x)=\frac{1}{2}(\gamma_{j,1}x_1^2+\gamma_{j,2}x_2^2)$ is the trapping potential with $0\leqslant\gamma_{j,1}\leqslant\gamma_{j,2}$, which is isotropic if $\gamma_{j,1}=\gamma_{j,2}$, otherwise it is called nonisotropic. The coefficients $\mu_j>0$ are for self-defocusing in the jth component of the beam, the coupling constant β_{ij} is the interaction between the ith and the jth components of the beam. The interaction of any two components is attractive if $\beta_{ij}<0$, and repulsive if $\beta_{ij}>0$. Eq. (1) also describes a physical model in which M-species Bose–Einstein condensates (BEC) come from ultra-cold dilute bosonic atoms in a magnetically trapped gas. Experimental reports concerning the BEC can be found, e.g., in [8,9,17,26]. Specifically, Hall et al. [26] reported the first experimental results concerning the dynamics of a two-component system of BEC in the different spin states of ^{87}Rb. For simplicity we denote a single nonlinear Schrödinger equation (NLS) by choosing $M=1$ in Eq. (1).

Eq. (1) has been studied extensively for many years because of their importance in many physical and mathematical problems; see e.g. [5]. Research articles concerning numerical solutions of Eq. (1) can be found, e.g., in [3,11,12,15,32–34,36]. For instance, Muruganandam and Adhikari [34] presented pseudospectral and finite difference methods for the numerical solution of the BEC in three dimensions. Bao and Tang [15] studied the ground-state solution of the BEC by directly minimizing the energy functional. To find the time-dependent solutions of Eq. (1), in general one has to discretize the partial derivatives $\frac{\partial}{\partial t}\Phi_j$, e.g., using the Crank–Nicolson finite difference (CNFD) scheme [2]. Bao et al. [13,14] developed time-splitting spectral approximations for the numerical solutions of Eq. (1), where the Fourier spectral method is used to discretize the Laplacian, and $\frac{\partial}{\partial t}\Phi_j$ are integrated exactly. Recent studies for the numerical solution of the GPE can be found in [23,38,40]. Specifically, Chin and Krotscheck [23] described a fourth-order algorithm for solving the imaginary time GPE in a rotation anisotropic trap. Wang [40] studied the split-step finite difference method for the numerical solution of the NLS.

The purpose of this paper is twofold. First, we wish to indicate that the numerical continuation methods described in [18,20] can be exploited to compute wave functions of Eq. (1). More precisely, let

$$\Phi_j(x,t)=\mathrm{e}^{-\mathrm{i}\lambda_j t}u_j(x), \quad j=1,\ldots,M, \tag{2}$$

where λ_j is the chemical potential, and $u_j(x)$ is a real function independent of time. Then Eq. (1) is transformed into M steady-state coupled NLS of the following form:

$$\begin{aligned} &-\Delta u_j - \lambda_j u_j + V_j(x)u_j + \mu_j u_j^3 + \sum_{i\neq j}\beta_{ij}u_i^2u_j = 0 \quad \text{in } \mathbf{R}^2,\\ &u_j>0 \quad \text{in } \mathbf{R}^2, \quad j=1,\ldots,M,\\ &u_j(x)\to 0 \quad \text{as } |x|\to+\infty. \end{aligned} \tag{3}$$

By the Hartree–Fock theory for BEC, we rewrite Eq. (3) as

$$\begin{aligned} &-\Delta u_j - \lambda_j u_j + V_j(x)u_j + \mu_j u_j^3 + \sum_{i\neq j}\beta_{ij}u_i^2u_j = 0 \quad \text{in } \Omega, \quad j=1,\ldots,M,\\ &u_1=u_2=\cdots=u_M=0 \quad \text{on } \partial\Omega. \end{aligned} \tag{4}$$

To be consistent with the physical meaning of Eq. (1), we assume that Ω is the unit disk in $\mathbf{R}^2$, see e.g. [27]. Eq. (4) is a nonlinear system of M equations of the following form:

$$F_j(u_1,\ldots,u_M,\lambda_j,\mu_j,\beta_{1j},\ldots,\beta_{j-1,j},\beta_{j+1,j},\ldots,\beta_{Mj})=0, \quad j=1,\ldots,M, \tag{5}$$

where F_j: $B_1\times\mathbf{R}^{M+1}\to B_2$ and $F(\cdot)=(F_1(\cdot),\ldots,F_M(\cdot))$, and B_1 and B_2 are two Banach spaces. For simplicity we keep the coefficients of the cubic terms fixed, and denote a point on the solution manifolds of Eq. (5) by $\{(u_j,\lambda_j)\}_{j=1:M}$. For $M=3$ Eq. (4) can be expressed as

$$\begin{aligned} &-\Delta u_1 - \lambda_1 u_1 + V_1(x)u_1 + \mu_1 u_1^3 + \beta_{21} u_1 u_2^2 + \beta_{31} u_1 u_3^2 = 0,\\ &-\Delta u_2 - \lambda_2 u_2 + V_2(x)u_2 + \mu_2 u_2^3 + \beta_{12} u_2 u_1^2 + \beta_{32} u_2 u_3^2 = 0 \quad \text{in } \Omega,\\ &-\Delta u_3 - \lambda_3 u_3 + V_3(x)u_3 + \mu_3 u_3^3 + \beta_{13} u_3 u_1^2 + \beta_{23} u_3 u_2^2 = 0,\\ &u_1 = u_2 = u_3 = 0 \quad \text{on } \partial\Omega. \end{aligned} \tag{6}$$

Next, we will show that the energy levels of a quantum particle governed by the Schrödinger eigenvalue problem (SEP)

$$\begin{aligned} &-\Delta u - \lambda u + V(x)u = 0 \quad \text{in } \Omega,\\ &u = 0 \quad \text{on } \partial\Omega \end{aligned} \tag{7}$$

correspond to the eigenvalues of the SEP. Since the eigenvalues of the SEP are just bifurcation points of the NLS without angular momentum term or damping term, it is clear that the energy level of the SEP can used as an initial guess to computing their counterpart of the NLS, where the continuation method is regarded as an iterative scheme. In other words, we may study the ground-state or other excited-state solutions of the MCNLS from the viewpoint of bifurcation. We remark here that Bao et al. [12–14] also used the eigenpairs of the SEP without boundary conditions as initial guesses to computing wave functions of the NLS.

We discretize Eq. (5) via centered difference approximations. To overcome the polar coordinate singularity at the origin, we exploit a technique in [31]. One can use a predictor–corrector continuation method [7,10,29] to trace solution curves and surfaces of Eq. (4), where one of the chemical potentials, say λ_1, is treated as the first continuation parameter. The advantage of this choice is that λ_1 can be easily obtained if the solution curve is numerically traced [18,20]. The other chemical potentials also can be used as the second continuation parameter and so on. If a solution curve of Eq. (4) branching from the first bifurcation point, say, $(0, \lambda_{0,1})$ is numerically traced, we obtain discrete points $\{(u_j, \lambda_j)\}_{j=1:M}$ on the solution curve, where $\lambda_2, \ldots, \lambda_M$ are fixed positive constants, and the continuation parameter $\lambda_1 > \lambda_{0,1}$ or $\lambda_1 < \lambda_{0,1}$ depending on the bifurcation is supercritical or subcritical. Actually, one may choose $\lambda_1 = \lambda_2$ or $\lambda_1 = \lambda_3$ and so on.

Now the wave functions $\Phi_j(x,t) = \mathrm{e}^{-\mathrm{i}\lambda_j t} u_j(x)$ can be easily obtained for any $t > 0$ and for the above-mentioned chemical potentials. To obtain $\Phi_j(x,t)$ for any different values of $\lambda_j, j = 2, \ldots, M$, we can treat, say λ_2, as the second continuation parameter, and keep the remaining chemical potentials $\lambda_3, \ldots, \lambda_M$ fixed. We repeat the process mentioned above until the $M-1$ two-dimensional surfaces with continuation parameters $(\lambda_1, \lambda_2), (\lambda_1, \lambda_3), \ldots, (\lambda_1, \lambda_M)$ are numerically traced. The algorithm is parallel because we can trace each solution surface simultaneously. We remark here that using a numerical continuation method to trace solution surfaces of parameter-dependent problems was described in [19]. It is inexpensive to implement the algorithm because in practical computations we only need to know the informations of some specific points on the solution surfaces. Additionally, the proposed algorithm has the following advantages: (i) It is unnecessary to discretize or integrate the left hand side of Eq. (1), namely, $\frac{\partial}{\partial t}\Phi_j(x,t)$. (ii) We can compute $\Phi_j(x,t)$ for any time scale and for any points $\{(u_j, \lambda_j)\}_{j=1:M}$ on the solution manifolds of $F(\cdot) = 0$.

Two important physical invariants of the MCNLS are the mass conservation constraints of the wave functions and the energy conservation. The former means that we need to impose the normalization conditions

$$\int_\Omega |u_j(x)|^2 \, \mathrm{d}x = 1, \quad j = 1, \ldots, M \tag{8}$$

on Eq. (4). From the viewpoint of computational cost, the normalization conditions are really a benefit to the numerical continuation for solving Eq. (4). First of all, the goal of tracing solution curves becomes clear. To be precise, we are only interested in at most M points $\{(u_j, \lambda_{1,j})\}_{j=1:M}$ with $\|u_j\|_2 = 1$ on the solution curves, where $\lambda_{1,j}$ denote different values of the continuation parameter λ_1 with respect to $\|u_j(x)\|_2 = 1$. This is because for any $j \neq k \in \{1, \ldots, M\}$, the components u_j and u_k might satisfy Eq. (8) for different values of λ_1 if we treat λ_1 as the continuation parameter. This fact may also explain the "phase separation" of the system. Next, since we are only interested in at most M points on the solution curve, we can choose a stepsize in the continuation algorithm as large as possible. Finally, we obtain the ground-state of the system by tracing solution curves branching from the first bifurcation point.

This paper is organized as follows. In Section 2, we analyze the relationship among the energy levels of a quantum particle, the associated eigenvalues of the SEP and the corresponding bifurcations of the NLS without angular momentum or damping term. Moreover, we apply the Liapunov–Schmidt reduction [24] to show that the simple bifurcation of a single NLS is pitchfork. The pitchfork bifurcation can be supercritical or subcritical, depending on the coefficient of the cubic term we choose. In Section 3, we discuss the centered difference approximations for two-coupled NLS. A parallel two-grid centered difference discretization scheme with two-loop continuation algorithm is described to computing steady states and wave functions of the MCNLS. Our numerical results are reported in Section 5. The test problems include a single, two- and three-coupled NLS, where the physical properties of the system such as mass conservation constraints, strong and weak repulsive interactions, and isotropic and nonisotropic trapping potentials are imposed. Finally, some concluding remarks are given in Section 6.

2. Energy level, eigenvalue and bifurcation

We will show that the energy levels of a quantum particle governed by the SEP correspond to its eigenvalues. On the other hand, the eigenvalues of the SEP are bifurcation points of the NLS on the trivial solution curve $\{(0,\lambda)|\lambda \in \mathbf{R}\}$ if the chemical potential λ is treated as a continuation parameter. Therefore, it is clear that one can use the energy level of the quantum particle as an initial guess to approximate their counterpart governed by the NLS, where the continuation method is used as the iterative scheme.

2.1. Linear stability and energies

Let $\Omega = \{(x_1,x_2) \in \mathbf{R}^2 : x_1^2 + x_2^2 < a^2\}$ be a circle of radius a in $\mathbf{R}^2$. We consider a quantum particle of mass M moving nonrelativistically in Ω. The wave function $u(x_1,x_2)$ of the particle is a solution of the 2D Schrödinger equation

$$\begin{aligned} &\Delta u = \frac{2M}{\hbar^2}[V(x) - E]u \quad \text{in } \Omega, \\ &u = 0 \quad \text{on } \partial\Omega, \end{aligned} \tag{9}$$

where $V(x)$ is the particle's potential energy, $\hbar$ is the Planck's constant, and E the total energy. The potential energy obeys Hooke's law and has the following form:

$$V(x) = \frac{1}{2}(\gamma_1 x_1^2 + \gamma_2 x_2^2)$$

for some constants $\gamma_1,\gamma_2 > 0$. Eq. (9) is also known as the Schrödinger eigenvalue problem (SEP). If we set $V(x) = 0$ in Eq. (9), then the Schrödinger equations reduces to

$$\begin{aligned} &\Delta u = -k^2 u \equiv -\lambda u \quad \text{in } \Omega, \\ &u = 0 \quad \text{on } \partial\Omega, \end{aligned} \tag{10}$$

where $k = \frac{\sqrt{2ME}}{\hbar}$. Now we consider the particle moving under the influence of a central force. A well known example is the hydrogen atom, in which the electron is held to the proton by the central Coulomb force. Then the wave function $u(x_1,x_2)$ can be expressed as a function of polar coordinates (r,θ). Using the technique of separation of variables $u(r,\theta) = v(r)z(\theta)$, the wave functions or eigenfunctions of Eq. (10) are

$$u_{m,n} = J_m\left(\frac{j_{m,n}r}{a}\right)[\alpha\cos m\theta + \beta \sin m\theta] \tag{11}$$

with eigenvalues

$$\lambda_{m,n} = \left(\frac{j_{m,n}}{a}\right)^2, \quad m = 0, \pm 1, \pm 2, \ldots. \tag{12}$$

Here $j_{m,n}$ is the nth zero of the mth Bessel function,

$$J_m(j_{m,n}) = 0,$$

where

$$J_m(z) = \frac{z^m}{2^m}\sum_{k=0}^{\infty}(-1)^k\frac{z^{2k}}{2^{2k}k!\Gamma(m+k+1)}, \quad |\arg z| < \pi$$

are solutions of the differential equation

$$\frac{d^2Z_m}{dz^2} + \frac{1}{z}\frac{dZ_m}{dz} + \left(1 - \frac{m^2}{z^2}\right)Z_m = 0,$$

and α, β arbitrary constants. We have asymptotically [30]

$$j_{m,n} \sim \left(n + \frac{m}{2} - \frac{1}{4}\right)\pi \quad \text{as } n \to \infty.$$

Eqs. (9) and (10) represent the particle have momentum

$$p_{\text{tang}} = \hbar\frac{k}{r}$$

in the direction tangential to the circle Ω, and the corresponding angular momentum is

$$L = p_{\text{tang}}r = k\hbar. \tag{13}$$

From Eqs. (10) and (12) we have

$$E_{m,n} = \frac{\hbar^2k^2}{2M} = \frac{\hbar^2\lambda_{m,n}}{2M}. \tag{14}$$

Eq. (14) shows that the energy levels of the system depend on the quantum numbers m and n. Since $E_{m,n} = E_{-m,n}$, there are two states with the same energy level except $m = 0$. Thus the energy level $E_{m,n}$ is two-fold degenerate, while the ground-state energy $E_{0,1}$ corresponding to the minimum eigenvalue $\lambda_{0,1}$ is nondegenerate. We may interpret this phenomenon using the concept of symmetric groups.

Without loss of generality, we choose $a = 1$ in our discussions given below. The first six eigenvalues of Eq. (10) are $\lambda_{0,1} \approx 5.78318596$, $\lambda_{1,1} \approx 14.68200152$, $\lambda_{2,1} \approx 26.37459278$, $\lambda_{0,2} \approx 30.47126234$, $\lambda_{3,1} \approx 40.70644163$, $\lambda_{1,2} \approx 49.2185030481$; see [1, p. 465]. As we can see from Eq. (11), the eigenvalues of Eq. (10) have geometric multiplicity two except $\lambda_{0,1}$. For instance, the set

$$J_1(j_{1,1}r)\cdot\text{span}\{\cos\theta, \sin\theta\} \tag{15}$$

constitutes a two-dimensional basis for the eigenspace corresponding to $\lambda_{1,1}$. Alternatively, if we choose $\alpha,\beta > 0$, then the set

$$J_1(j_{1,1}r)\cdot\text{span}\{\alpha\cos\theta - \beta\sin\theta, \alpha\cos\theta + \beta\sin\theta\} \tag{16}$$

is another two-dimensional basis for the same eigenspace. Let $O(n)$ denote the n-dimensional orthogonal group, i.e.,

$$O(n) = \{A \in \mathbf{R}^{n\times n} | AA^T = I_n\}$$

is the set of all $n \times n$ orthogonal matrices. In particular,

$$O(2) = \left\{\begin{bmatrix}\cos\theta & -\sin\theta\\ \sin\theta & \cos\theta\end{bmatrix}, \begin{bmatrix}\cos\theta & \sin\theta\\ \sin\theta & -\cos\theta\end{bmatrix}\middle| \theta \in [0, 2\pi)\right\},$$

which consists of rotations and reflections of $\mathbf{R}^2$ that keeps the origin fixed. Thus, the circle group

$$S^1 = \left\{\begin{bmatrix}\cos\theta & -\sin\theta\\ \sin\theta & \cos\theta\end{bmatrix}\middle| \theta \in [0, 2\pi)\right\}$$

is a subgroup of O(2). The special orthogonal group $SO(n)$ consists of all $A \in \mathrm{O}(n)$ such that $\det A = 1$. In particular, $SO(2)$ consists of the planar rotations, either clockwise or counterclockwise. Thus, $SO(2) = S^1$. We refer to [25, Chapter 11] for details. It is obvious that the basis (16) is invariant under the action of S^1. Therefore, the eigenspace corresponding to the eigenvalues of Eq. (10) are two-dimensional except the first one.

To determine the energy levels of Eq. (9), we have to find the eigenpairs, which can be obtained using numerical methods. We will give a detailed discussion in Section 2.2.

2.2. Local bifurcation analysis at simple eigenvalues

Recently, Chang and Chien [20] applied the Liapunov–Schmidt reduction to show that the simple bifurcations of a single NLS defined on a unit interval (square) are pitchfork. The pitchfork bifurcation can be supercritical or subcritical depending on the coefficient of the cubic term we choose. We will show that similar results hold if the domain Ω is a disk.

Let $\mathscr{E}_{x,\lambda}$ be the space of all functions g: $\mathbf{R}^2 \to \mathbf{R}$ that are defined and C^∞ on some neighborhood of the origin. We identify any two functions in $\mathscr{E}_{x,\lambda}$ which are equal as germs. Let $g, h \in \mathscr{E}_{x,\lambda}$. We say that g and h are strongly equivalent if there exist functions $X(x,\lambda)$ and $S(x,\lambda)$ such that the relation $g(x,\lambda) = S(x,\lambda)h(X(x,\lambda),\lambda)$ holds near the origin. The following result can be found in [24, p. 95].

Proposition 2.1. *A germ $g \in \mathscr{E}_{x,\lambda}$ is strongly equivalent to $\alpha x^k + \beta\lambda x$ if and only if at $(x,\lambda) = (0,0)$,*

$$g = \frac{\partial}{\partial x}g = \cdots = \left(\frac{\partial}{\partial x}\right)^{k-1} g = \frac{\partial}{\partial \lambda}g = 0 \quad \text{and} \quad \alpha = \operatorname{sign}\left(\frac{\partial}{\partial x}\right)^k g, \beta = \operatorname{sign}\frac{\partial}{\partial \lambda}\frac{\partial}{\partial x}g.$$

For simplicity we rewrite Eq. (5) as $F(u,\lambda) = 0$, where $u = (u_1, \ldots, u_M)$ and $\lambda = \lambda_1$. That is, the parameters in Eq. (4) are fixed except λ_1. Let L be the differential of F with respect to $(u,\lambda) = (0,0)$, i.e., $L = (dF)_{0,0} = F_u(0,0)$. Note that L is a differential operator of index 0. Let B_1 and B_2 be the Banach spaces defined in Eq. (5). The Liapunov–Schmidt reduction is briefly described as follows:

Step 1. Decompose

$$\text{(a) } B_1 = \ker L \oplus M \quad \text{and} \quad \text{(b) } B_2 = N \oplus R(L), \tag{17}$$

where $\ker L$ and $R(L)$ denote the kernel and the range of L, respectively.

Step 2. Split Eq. (5) into an equivalent pair of equations:

$$\text{(a) } EF(u,\lambda) = 0, \quad \text{(b) } (I-E)F(u,\lambda) = 0, \tag{18}$$

where E: $B_2 \to R(L)$ is the projection associated to the splitting.

Step 3. Use Eq. (17)a to write $u = v + w$, where $v \in \ker L$ and $w \in M$. Define a map G: $\ker L \times M \times \mathbf{R} \to R(L)$ from Eq. (18)a by

$$G(v,w,\lambda) = EF(v+w,\lambda). \tag{19}$$

The differential of G with respect to w at the origin is

$$EL = L.$$

Since the operator L is Fredholm, $R(L)$ is closed. Therefore,

$$L : M \to R(L)$$

is invertible. Apply the implicit function theorem to solve Eq. (18)a for w as a function of v and λ. This leads to a function W, W: $\ker L \times \mathbf{R} \to M$ such that

$$EF(v + W(v,\lambda),\lambda) = 0. \tag{20}$$

Step 4. Define ϕ: $\ker L \times \mathbf{R} \to N$ by

$$\phi(v_0,\lambda) = (I-E)F(xv_0 + W(xv_0,\lambda),\lambda). \tag{21}$$

Note that the vector in Eq. (20) is replaced by xv_0, $x \in \mathbf{R}$ in Eq. (21).

Step 5. Choose a basis v_0^* for $(R(L))^{\perp}$. Define g: $\mathbf{R}\times\mathbf{R}\to\mathbf{R}$ by

$$g(x,\lambda)=\langle v_0^*, F(xv_0+W(xv_0,\lambda),\lambda)\rangle,$$

where $\langle r,s\rangle=\int_\Omega r(\xi)s(\xi)\,\mathrm{d}\xi$. Since L is self adjoint, we have $L=L^*$ and so $v_0^*=v_0$. Since F is an odd function with respect to u, we have $(d^2F)_{0,\lambda}=\mathrm{O}$ and $F_\lambda=\mathrm{O}$, where O denotes the zero operator. Thus at the bifurcation point $(0,\lambda_{m,n})$, the reduced function g satisfies $g=g_x=g_{xx}=g_\lambda=0$. We refer to [24, Chapters 1 and 7] for details.

Theorem 2.2. *The first bifurcation of*

$$\begin{aligned} &-\Delta u-\lambda u+\mu u^3=0 \quad \text{in } \Omega,\\ &u=0 \quad \text{on } \partial\Omega \end{aligned} \tag{22}$$

is pitchfork. Moreover, the pitchfork bifurcation is supercritical if $\mu>0$, and subcritical if $\mu<0$, where Ω is the unit disk.

Proof. Let F: $X\times\mathbf{R}\to C^0(\Omega)$ be the mapping defined by

$$F(u,\lambda)=-\Delta u-\lambda u+\mu u^3,$$

where $X=\{u\in C^2(\Omega)\colon u=0 \text{ on } \partial\Omega\}$. Note that the linear operator $L=(dF)_{0,\lambda}=-\Delta-\lambda$ is singular at $\lambda=\lambda_{0,1}$. It has a one-dimensional kernel spanned by $u_{0,1}$, where $u_{0,1}$ and $\lambda_{0,1}$ are defined in Eqs. (11) and (12), respectively. To prove that the first bifurcation of Eq. (22) is pitchfork, we only need to compute

$$g_{xxx}=\langle u_{0,1},(d^3F)_{0,\lambda_{0,1}}(u_{0,1},u_{0,1},u_{0,1})\rangle, \tag{23}$$

and

$$g_{\lambda x}=\langle u_{0,1},(dF_\lambda)_{0,\lambda_{0,1}}\cdot u_{0,1}\rangle. \tag{24}$$

By definition,

$$(d^3F)_{0,\lambda_{0,1}}(u_{0,1},u_{0,1},u_{0,1})=\frac{\partial}{\partial t_1}\frac{\partial}{\partial t_2}\frac{\partial}{\partial t_3}F(0+t_1u_{0,1}+t_2u_{0,1}+t_3u_{0,1},\lambda_{0,1})\Big|_{t_1=t_2=t_3=0}=6\mu u_{0,1}^3. \tag{25}$$

Substituting Eq. (25) into Eq. (23) yields

$$g_{xxx}=\langle u_{0,1},6\mu u_{0,1}^3\rangle=6\mu\int_\Omega u_{0,1}^4\neq 0 \quad \text{when } \mu\neq 0.$$

Similarly, $F_\lambda(u,\lambda)=-u$, and we have

$$(dF_\lambda)_{0,\lambda_{0,1}}\cdot u_{0,1}=\frac{\mathrm{d}}{\mathrm{d}t}F_\lambda(0+tu_{0,1},\lambda_{0,1})|_{t=0}=-u_{0,1}. \tag{26}$$

Thus,

$$g_{\lambda x}=\langle u_{0,1},-u_{0,1}\rangle=-\int_\Omega u_{0,1}^2<0.$$

From which it follows that the reduced function g is equivalent to the normal form $\alpha x^3-\lambda x=0$ where $\alpha=sign(\mu)$. Thus the first bifurcation of Eq. (22) is pitchfork. Moreover, the pitchfork bifurcation is supercritical if $\mu>0$, and subcritical if $\mu<0$. □

Remark 2.3. Actually, Theorem 2.2 holds for the other bifurcations of Eq. (22).

Now we consider a single NLS

$$\begin{aligned} &\mathrm{i}\varepsilon\Phi_t=-\frac{\varepsilon^2}{2}\Delta\Phi+V(x)\Phi+\mu|\Phi|^2\Phi, \quad t>0,\ x\in\Omega\subseteq\mathbf{R}^2,\\ &\Phi(x,t)=0, \quad x\in\partial\Omega,\ t\geqslant 0. \end{aligned} \tag{27}$$

We say that the system has strong repulsive interaction if $\varepsilon = o(1)$, and weak repulsive interaction if $\varepsilon = O(1)$. Two important invariants of (27) are the mass conservation constraint of the wave function

$$N(\Phi) = \int_\Omega |\Phi(x,t)|^2 \, dx = 1, \quad t \geqslant 0, \tag{28}$$

and the energy conservation

$$E_\mu(\Phi) = \int_\Omega \left[\frac{\varepsilon^2}{2} |\nabla \Phi(x,t)|^2 + V(x)|\Phi(x,t)|^2 + \frac{\mu}{2}|\Phi(x,t)|^4 \right] dx, \quad t \geqslant 0. \tag{29}$$

Setting $\Phi(x,t) = e^{-i\lambda t/\varepsilon} u(x)$ in Eq. (27), we obtain the following semilinear elliptic eigenvalue problem:

$$\begin{aligned} &\lambda u(x) = -\frac{\varepsilon^2}{2}\Delta u(x) + V(x)u(x) + \mu u(x)^3 \quad \text{in } \Omega, \\ &u(x) = 0 \quad \text{on } \partial\Omega, \end{aligned} \tag{30}$$

for $u(x)$ under the normalization condition

$$\int_\Omega |u(x)|^2 \, dx = 1. \tag{31}$$

It is obvious that any eigenvalue λ can be computed from its corresponding eigenfunction $u(x)$ by

$$\lambda = \lambda_\mu(u) = \int_\Omega \left[\frac{\varepsilon^2}{2}|\nabla u(x)|^2 + V(x)|u(x)|^2 + \mu |u(x)|^4 \right] dx = E_\mu(u) + \int_\Omega \frac{\mu}{2}|\phi(x)|^4 \, dx. \tag{32}$$

Let $\{v_1, v_2, \ldots,\}$ denote the eigenvalues of the Schrödinger eigenvalue problem

$$\begin{aligned} &-\frac{\varepsilon^2}{2}\Delta u(x) + V(x)u(x) = \lambda u(x) \quad \text{in } \Omega, \\ &u(x) = 0 \quad \text{on } \partial\Omega. \end{aligned} \tag{33}$$

It is clear that the bifurcations of Eq. (30) are located at $\{(0,v_1),(0,v_2),\ldots,\}$. Here and in the sequel, unless otherwise specified we omit the symbol ε^2 in our discussions. We will show that the first bifurcation scenario of a single NLS is the same as that of Eq. (22).

Theorem 2.4. *The first bifurcation of Eq. (30) is pitchfork. Moreover, the pitchfork bifurcation is supercritical if* $\mu > 0$, *and subcritical if* $\mu < 0$.

Proof. Let F: $X \times \mathbf{R} \to C^0(\Omega)$ be the mapping defined by

$$F(u,\lambda) = -\frac{1}{2}\Delta u + Vu - \lambda u + \mu u^3,$$

where $X = \{u \in C^2(\Omega) : u = 0 \text{ on } \partial\Omega\}$. Note that the linear operator $L = (dF)_{0,\lambda} = -\frac{1}{2}\Delta + V - \lambda$ is singular at $\lambda = v_1$, and it has a one-dimensional kernel spanned by u_1, where u_1 and v_1 is the first eigenpair of Eq. (33). To prove that the first bifurcation of Eq. (30) is pitchfork, we only need to compute

$$g_{xxx} = \langle u_1, (d^3F)_{0,v_1}(u_1,u_1,u_1)\rangle \quad \text{and} \quad g_{\lambda x} = \langle u_1, (dF_\lambda)_{0,v_1} \cdot u_1 \rangle.$$

By definition,

$$\begin{aligned} &(d^3F)_{0,v_1}(u_1,u_1,u_1) = \frac{\partial}{\partial t_1}\frac{\partial}{\partial t_2}\frac{\partial}{\partial t_3} F(0 + t_1u_1 + t_2u_1 + t_3u_1, v_1)\Big|_{t_1=t_2=t_3=0} = 6\mu u_1^3, \\ &(dF_\lambda)_{0,v_1} \cdot u_1 = \frac{d}{dt} F_\lambda(0 + tu_1, v_1)\Big|_{t=0} = -u_1. \end{aligned} \tag{34}$$

Note that Eq. (34) has the same form as that of Eqs. (25) and (26). The remainder of the proof is the same as that of Theorem 2.2, and is omitted here. □

Note that the eigenvalues of Eq. (33) can only be obtained using numerical methods. We observe that if the trapping potential $V(x)$ is nonisotropic, then the double eigenvalues of Eq. (33) will be split into two simple ones, and this property is independent of the geometries of the domain. To be precise, let $V(x) = \frac{1}{2}(\gamma_1^2 x_1^2 + \gamma_2^2 x_2^2)$, and μ_j, μ_{j+1} denote two clustered eigenvalues, then $|\mu_j - \mu_{j+1}|$ increases as $|\gamma_1^2 - \gamma_2^2|$ increases. Therefore, we can apply the Liapunov–Schmidt reduction to analyze the local bifurcation behavior of the NLS. We used the function "eig" in MATLAB to compute the first six eigenvalues of Eq. (33) with various choices of trapping potentials, where the equation is discretized by the centered difference approximations described in Section 3 with radial meshsize $\Delta r = \frac{2}{201}$ and azimuthal size $\Delta\theta = \frac{2\pi}{72}$. From Table 1 we obtain the following result.

Proposition 2.5. *If the trapping potential $V(x)$ in Eq. (30) is nonisotropic, then all bifurcations are simple. Moreover, all bifurcations of Eq. (30) are pitchfork. The pitchfork bifurcation can be supercritical or subcritical depending on $\mu > 0$ or $\mu < 0$.*

Proposition 2.5 shows an interesting fact that the degenerate energy levels of a quantum particle will not be preserved if the trapping potential is nonisotropic.

2.3. Mode interactions

Now we consider the two-coupled NLS in one dimension

$$\begin{aligned} &-\Delta u - \lambda_1 u + \mu_1 u^3 + \beta u v^2 = 0, \\ &-\Delta v - \lambda_2 v + \mu_2 v^3 + \beta u^2 v = 0 \quad \text{in } \Omega_1 = (0,\ell), \\ &u = v = 0 \quad \text{on } \partial\Omega_1. \end{aligned} \tag{35}$$

A change of variable $x = \ell\tilde{x}$ transforms the domain Ω_1 in (35) back to $\Omega = (0,1)$ again. By using the same notations as before, Eq. (35) can be expressed as

$$\begin{aligned} &-\frac{1}{\ell^2}\Delta u - \lambda_1 u + \mu_1 u^3 + \beta u v^2 = 0, \\ &-\frac{1}{\ell^2}\Delta v - \lambda_2 v + \mu_2 v^3 + \beta u^2 v = 0 \quad \text{in } \Omega = (0,1), \\ &u = v = 0 \quad \text{on } \partial\Omega. \end{aligned} \tag{36}$$

Now we consider the case $\lambda_1 = \lambda_2 = \lambda$. Let $C_0^2(\Omega) := \{u \in C^2(\Omega) | u|_{\partial\Omega} = 0\}$, $X = (C_0^2(\Omega))^2$, and $w = (u, v)$. We use the same nonlinear mapping F for Eq. (36) as in Section 1. The differential of F evaluated at $w = (0,0)$ is

Table 1
The first six eigenvalues of Eq. (33) with various choices of trapping potentials and $\frac{\varepsilon^2}{2} = 1$

	$V(x) = 0$	$V(x) = x_2^2/2$	$V(x) = (x_1^2 + x_2^2)/2$
1	5.7828623159990	5.8382345626141	5.8936910922701
2	14.6776718955286	14.7199222170310	14.8468449336785
3	14.6776718956579	14.8045086340521	14.8468449337180
4	26.3394222468847	26.4423977042872	26.5468641734112
5	26.3394222468847	26.4430854926601	26.5468641734314
6	30.4633511101872	30.5431869224575	30.6215793901315
	$V(x) = (2x_1^2 + x_2^2)/2$	$V(x) = (3x_1^2 + x_2^2)/2$	$V(x) = (4x_1^2 + x_2^2)/2$
1	5.9487476448496	6.0034097436138	6.0576828341890
2	14.8889736894021	14.9308971016107	14.9726173416088
3	14.9733158306247	15.0993369017885	15.2249101499556
4	26.6496488101970	26.7507184328762	26.8500436174623
5	26.6503487078572	26.7535404623676	26.8564408010334
6	30.7015176130202	30.7830308174554	30.8661445675133

$$L = (d_w \Phi)_{0,0,\lambda} = \begin{pmatrix} -\frac{1}{\ell^2}\Delta - \lambda & 0 \\ 0 & -\frac{1}{\ell^2}\Delta - \lambda \end{pmatrix}. \tag{37}$$

It is obvious that the domain X of the linear operator L can be decomposed as

$$X = \sum_{k=1}^{\infty} \oplus X_k, \quad X_k := \left\{ \begin{pmatrix} c_1 \\ c_2 \end{pmatrix} \sin k\pi x \middle| c_1, c_2 \in \mathbf{R} \right\}, \quad k \in \mathbf{N}, \tag{38}$$

and the operator L maps X_k into itself. The restriction of L in the subspace X_k is a 2×2 matrix

$$M_k(\lambda, \ell) := L|_{X_k} = \begin{pmatrix} -\frac{k^2\pi^2}{\ell^2}\Delta - \lambda & 0 \\ 0 & -\frac{k^2\pi^2}{\ell^2}\Delta - \lambda \end{pmatrix}, \quad k = 1, 2, \ldots. \tag{39}$$

It is well known that a nonlinear system with multiple bifurcation parameters will have multiple modes. Since multiple eigenvalues may lead to secondary bifurcation, it is possible that secondary bifurcations may arise in the system. This process is called mode interactions [25, pp. 412–414]. Note that the 2×2 matrix $M_k(\lambda, \ell)$ in Eq. (39) involves two parameters λ and ℓ. However, it has been indicated in [20] that mode interactions can not occur in Eq. (36). The same result holds if we consider the two-coupled NLS defined on the unit square or unit disk. We can exploit the modified Liapunov–Schmidt reduction described in [16] to study the local bifurcation behavior of the two coupled NLS. The details will be given elsewhere.

3. Centered difference approximations on the unit disk

3.1. Two-coupled nonlinear Schrödinger equations on a unit disk

Without loss of generality, we consider the two-coupled NLS

$$\begin{aligned} &-\Delta u_1 - \lambda_1 u_1 + V_1(x)u_1 + \mu_1 u_1^3 + \beta u_2^2 u_1 = 0 \quad \text{in } \Omega, \\ &-\Delta u_2 - \lambda_2 u_2 + V_2(x)u_2 + \mu_2 u_2^3 + \beta u_1^2 u_2 = 0 \quad \text{in } \Omega, \\ &u_1 = u_2 = 0 \quad \text{on } \partial\Omega, \end{aligned} \tag{40}$$

where $\Omega = \{(x_1, x_2) : x_1^2 + x_2^2 < 1\}$ is the unit disk. It is natural to apply the polar coordinate transformations $x_1 = r\cos\theta$, $x_2 = r\sin\theta$ to Eq. (40). For simplicity, we use the same notations to represent the functions both in Cartesian and polar coordinates. The two-coupled NLS of $u_1(r,\theta)$ and $u_2(r,\theta)$ can be written as

$$\begin{aligned} &-\left(\frac{\partial^2 u_1}{\partial r^2} + \frac{1}{r}\frac{\partial u_1}{\partial r} + \frac{1}{r^2}\frac{\partial^2 u_1}{\partial \theta^2}\right) - \lambda_1 u_1 + V_1(r,\theta)u_1 + \mu_1 u_1^3 + \beta u_2^2 u_1 = 0 \quad \text{in } \Omega, \\ &-\left(\frac{\partial^2 u_2}{\partial r^2} + \frac{1}{r}\frac{\partial u_2}{\partial r} + \frac{1}{r^2}\frac{\partial^2 u_2}{\partial \theta^2}\right) - \lambda_2 u_2 + V_2(r,\theta)u_2 + \mu_2 u_2^3 + \beta u_1^2 u_2 = 0 \quad \text{in } \Omega, \\ &u_1(1,\theta) = u_2(1,\theta) = 0, \quad 0 \leqslant \theta \leqslant 2\pi. \end{aligned} \tag{41}$$

The centered difference approximations described in [31] is exploited to discretize Eq. (41) with $\Delta r = \frac{2}{2M+1}$ as the radial meshsize and $\Delta\theta = \frac{2\pi}{N}$ as the azimuthal meshsize for positive integers M and N. The locations of grid points are half-integers in radial direction and integers in azimuthal direction. That is,

$$r_i = \left(i - \frac{1}{2}\right)\Delta r, \quad \theta_j = (j-1)\Delta\theta \tag{42}$$

for $i = 1, 2, \ldots, M$ and $j = 1, 2, \ldots, N$.

Let $U_{i,j} = u_1(r_i, \theta_j)$, $V_{i,j} = u_2(r_i, \theta_j)$. We have the difference equations

$$-\left(\frac{U_{i+1,j} - 2U_{i,j} + U_{i-1,j}}{(\Delta r)^2} + \frac{1}{r_i}\frac{U_{i+1,j} - U_{i-1,j}}{2\Delta r} + \frac{1}{r_i^2}\frac{U_{i,j+1} - 2U_{i,j} + U_{i,j-1}}{(\Delta\theta)^2}\right) - \lambda_1 U_{i,j} + F_{i,j} = 0, \tag{43}$$

and

$$-\left(\frac{V_{i+1,j}-2V_{i,j}+V_{i-1,j}}{(\Delta r)^2}+\frac{1}{r_i}\frac{V_{i+1,j}-V_{i-1,j}}{2\Delta r}+\frac{1}{r_i^2}\frac{V_{i,j+1}-2V_{i,j}+V_{i,j-1}}{(\Delta\theta)^2}\right)-\lambda_1 V_{i,j}+G_{i,j}=0,$$
$$U_{M+1,j}=V_{M+1,j}=0, \tag{44}$$

where $F_{i,j}=V_1(r_i,\theta_j)U_{i,j}+\mu_1U_{i,j}^3+\beta V_{i,j}^2U_{i,j}$ and $G_{i,j}=V_2(r_i,\theta_j)V_{i,j}+\mu_2V_{i,j}^3+\beta U_{i,j}^2V_{i,j}$. Eqs. (43) and (44) can be expressed as

$$\begin{aligned}
&\frac{1}{(\Delta r)^2}\left[-\beta_iU_{i,j+1}+(2+2\beta_i)U_{i,j}-\beta_iU_{i,j-1}-(1-\alpha_i)U_{i-1,j}-(1+\alpha_i)U_{i+1,j}\right]+F_{i,j}=\lambda_1U_{i,j},\\
&\frac{1}{(\Delta r)^2}\left[-\beta_iV_{i,j+1}+(2+2\beta_i)V_{i,j}-\beta_iV_{i,j-1}-(1-\alpha_i)V_{i-1,j}-(1+\alpha_i)V_{i+1,j}\right]+G_{i,j}=\lambda_2V_{i,j},\\
&U_{M+1,j}=V_{M+1,j}=0,
\end{aligned} \tag{45}$$

where $\beta_i=\frac{1}{(i-\frac{1}{2})^2(\Delta\theta)^2}$, $\alpha_i=\frac{1}{2i-1}$, for $i=1,2,\ldots,M$ and $j=1,2,\ldots,N$.

Let $A\in\mathbf{R}^{MN\times MN}$ be the discretization matrix associated with the Laplacian $-\Delta$. Suppose that the unknown vectors U and V are represented by $U=[U_{11},\ldots,U_{1N},\ldots,U_{M1},\ldots,U_{MN}]^{\mathrm{T}}$, $V=[V_{11},\ldots,V_{1N},\ldots,V_{M1},\ldots,V_{MN}]^{\mathrm{T}}$, and $F=[F_{11},F_{12},\ldots,F_{MN}]^{\mathrm{T}}$, $G=[G_{11},G_{12},\ldots,G_{MN}]^{\mathrm{T}}$. From Eq. (45), we obtain

$$\begin{aligned}
&AU+F=\lambda_1U,\\
&AV+G=\lambda_2V,
\end{aligned} \tag{46}$$

where

$$A=\frac{1}{(\Delta r)^2}\begin{bmatrix}
2I+\beta_1\Phi & -(1+\alpha_1)I & & & \\
-(1-\alpha_2)I & 2I+\beta_2\Phi & -(1+\alpha_2)I & & \\
& \ddots & \ddots & \ddots & \\
& & -(1-\alpha_{M-1})I & 2I+\beta_{M-1}\Phi & -(1+\alpha_{M-1})I\\
& & & -(1-\alpha_M)I & 2I+\beta_M\Phi
\end{bmatrix} \tag{47}$$

with I the $N\times N$ identity matrix, and

$$\Phi=\begin{bmatrix}
2 & -1 & & & -1\\
-1 & 2 & -1 & & \\
& \ddots & \ddots & \ddots & \\
& & -1 & 2 & -1\\
-1 & & & -1 & 2
\end{bmatrix}\in\mathbf{R}^{N\times N}.$$

If we choose the radial direction first, and then the azimuthal direction. In this case the unknown vectors U and V are represented by

$$U=[U_{11},\ldots,U_{M1},\ldots,U_{1N},\ldots,U_{MN}]^{\mathrm{T}},\quad V=[V_{11},\ldots,V_{M1},\ldots,V_{1N},\ldots,V_{MN}]^{\mathrm{T}}.$$

Then the coefficient matrix associated with the Laplacian $-\Delta$ is

$$\widetilde{A}=\frac{1}{(\Delta r)^2}\begin{bmatrix}
\Psi & -B & & & -B\\
-B & \Psi & -B & & \\
& \ddots & \ddots & \ddots & \\
& & -B & \Psi & -B\\
-B & & & -B & \Psi
\end{bmatrix}, \tag{48}$$

where

$$\Psi = \begin{bmatrix} 2+2\beta_1 & -(1+\alpha_1) & & & \\ -(1-\alpha_2) & 2+2\beta_2 & -(1+\alpha_2) & & \\ & \ddots & \ddots & \ddots & \\ & & -(1-\alpha_{M-1}) & 2+2\beta_{M-1} & -(1+\alpha_{M-1}) \\ & & & -(1-\alpha_M) & 2+2\beta_M \end{bmatrix} \in \mathbf{R}^{M\times M},$$

and

$$B = \operatorname{diag}(\beta_1, \beta_2, \ldots, \beta_M).$$

Note that both the matrices A and $\widetilde{A}$ are nonsymmetric but nearly symmetric. Since A is a tridiagonal block matrix, one may use Gaussian elimination to solve the associated linear systems if the dimension of A is not too large. Alternatively, one also can use iterative methods such as Bi-CGSTAB [39] to solve linear systems with A and $\widetilde{A}$ as the coefficient matrices. We have the following result.

Lemma 3.1. *The matrices A and $\widetilde{A}$ in Eqs. (47) and (48), respectively, are similar.*

Proof. Let

$$P = \begin{bmatrix} P_1 \\ P_2 \\ \vdots \\ P_N \end{bmatrix}$$

with

$$P_j = \begin{bmatrix} e_j^{\mathrm{T}} \\ e_{N+j}^{\mathrm{T}} \\ \vdots \\ e_{(M-1)N+j}^{\mathrm{T}}, \end{bmatrix}, \quad j = 1, 2, \ldots, N,$$

where e_j is the j th column of the identity matrix. We can easily verify that $P\widetilde{A}P^{\mathrm{T}} = A$. Since P is a permutation matrix which is orthogonal, the result follows immediately. □

To prove that all the eigenvalues of $\widetilde{A}$ are strictly positive, we need the following result. We refer to [28, p. 363] for details.

Theorem 3.2 (Taussky). *Let $B \in \mathbf{R}^{n\times n}$ be irreducibly diagonally dominant. If B has only real eigenvalues, and if all main diagonal entries of B are strictly positive, then all the eigenvalues of B are strictly positive.*

The unsymmetry of the two matrices A and $\widetilde{A}$ are caused by the discretization scheme we use. We will show that the matrix $\widetilde{A}$ is similar to a symmetric one.

Theorem 3.3. *The matrix $\widetilde{A}$ is similar to a symmetric matrix, and all the eigenvalues of $\widetilde{A}$ are strictly positive.*

Proof. First we show $\widetilde{A}$ is similar to a symmetric matrix. Let $C = \operatorname{diag}(c_1, c_2, \ldots, c_M) \in \mathbf{R}^{M\times M}$ with $c_1 = 1$, $c_i = \sqrt{\frac{(1+\alpha_1)(1+\alpha_2)\cdots(1+\alpha_{i-1})}{(1-\alpha_2)(1-\alpha_3)\cdots(1-\alpha_i)}}$, $i = 2,3,\ldots,M$, and let

$$D = \operatorname{diag}\left(\underbrace{C, C, \ldots, C}_{N \text{ copies}}\right) \in \mathbf{R}^{MN\times MN}.$$

Then

$$D\widetilde{A}D^{-1} = \frac{1}{(\Delta r)^2}\begin{bmatrix} \widehat{\Psi} & -B & & & -B \\ -B & \widehat{\Psi} & -B & & \\ & \ddots & \ddots & \ddots & \\ & & -B & \widehat{\Psi} & -B \\ -B & & & -B & \widehat{\Psi} \end{bmatrix} := \widehat{A},$$

where $\widehat{A}$ is symmetric with

$$\widehat{\Psi} = \begin{bmatrix} 2+2\beta_1 & -\gamma_1 & & & \\ -\gamma_1 & 2+2\beta_2 & -\gamma_2 & & \\ & \ddots & \ddots & \ddots & \\ & & -\gamma_{M-2} & 2+2\beta_{M-1} & -\gamma_{M-1} \\ & & & -\gamma_{M-1} & 2+2\beta_M \end{bmatrix}$$

and $\gamma_i = \sqrt{(1+\alpha_i)(1-\alpha_{i+1})}$ for $i = 1, 2, \ldots, M-1$. Since $\widetilde{A}$ and $\widehat{A}$ are similar, all the eigenvalues of $\widetilde{A}$ are real. One can verify that $\widetilde{A}$ has the following three properties:

(a) $\widetilde{A}$ is irreducibly diagonally dominant,
(b) all main diagonal entries of $\widetilde{A}$ are strictly positive,
(c) $\widetilde{A}$ has only real eigenvalues.

By Taussky's theorem, we show that all the eigenvalues of $\widetilde{A}$ are strictly positive. □

Remark 3.4. As is well known, the spectral methods are widely used to discretize the Laplacian of nonlinear Schrödinger equations. It would be of interest to exploit the spectral methods in numerical continuation for curve-tracking. For instance, the spectral-Galerkin methods described in [37] can be used to discretize Eq. (40) defined in a unit disk or a cylindrical domain. The further study on this topic will be given elsewhere.

3.2. A two-grid discretization scheme

It is possible to develop a two-grid discretization method in the context of the centered difference approximations described in Section 3.1. Suppose that $\Delta\widetilde{r} = \frac{2}{2\widetilde{M}+1}$ is the radial meshsize on the coarse grid. To avoid the singularity at the origin, we have to choose $\Delta r = \frac{1}{3}\Delta\widetilde{r}$ as the radial meshsize on the fine grid. For instance, if $\widetilde{M} = 16$ and $\Delta\widetilde{r} = \frac{2}{33}$, then $\Delta r = \frac{2}{99} = \frac{2}{2M+1}$. That is, $M = 3\widetilde{M} + 1 = 49$. The details of the two-grid centered difference discretization scheme is similar to the one given in [21] and is omitted here. For $\Delta r = \frac{2}{33}$ and $\Delta\theta = \frac{2\pi}{16}$, the first eight eigenvalues of the discrete matrix are 5.771191, 14.578039, 14.578039, 25.636476, 25.636476, 30.178900, 37.953979, 37.953979, which shows that at least two simple eigenvalues exist. Moreover, both the geometric and algebraic multiplicities of the other eigenvalues are twofold.

4. Computing wave functions

4.1. The main algorithm

To compute the wave functions of Eq. (1), in general one has to discretize or integrate the partial derivatives $\mathrm{i}\frac{\partial\Phi_j}{\partial t}$, $j = 1, \ldots, M$. In this section we describe an algorithm which is different from the traditional methods. However, it can be used to compute $\Phi_j(x,t)$ efficiently. Actually, the idea behind our algorithm involves an "reversing process".

Remember Eq. (1) can be transformed into Eq. (4) via Eq. (2), namely,

$$\Phi_j(x,t) = \mathrm{e}^{-\mathrm{i}\lambda_j t}u_j(x).$$

Since Eq. (4) is a nonlinear system involving multi-parameters, we can apply a predictor–corrector continuation algorithm to trace the solution manifolds. From Eq. (2) it is clear that if the chemical potentials λ_j and the steady state solutions $u_j(x)$ are known, then the wave functions $\Phi_j(x,t)$ are readily available for any time t. Therefore, we treat λ_j as the continuation parameters and keep the other parameters in Eq. (4) fixed. We will combine the continuation algorithm described in [19] together with the two-grid discretization scheme in [21] to trace solution manifolds of Eq. (4). Suppose that we wish to trace the solution manifolds of Eq. (4) branching from the first bifurcation point.

Algorithm 4.1. Computing wave functions of the MCNLS: a two-grid scheme.

Input:

$\varepsilon :=$ accuracy tolerance of approximating points for the solution curves on both coarse and fine grids.

Step 0. $\lambda_1 :=$ the continuation parameter.
$\lambda_2, \ldots, \lambda_M :=$ constants.

Step 1. Outer continuation.
Use a predictor–corrector continuation algorithm to compute an approximating point on the coarse grid.

Step 2. Inner continuation.
(i) Predictor: Use the approximating point obtained in Step 1 as the predicted point.
(ii) Corrector. (a) Make a correction on the fine grid; (b). Perform Newton's method until $\|F(\cdot)\| < \varepsilon$.

Step 3. Go to Step 1 until the solution curve is traced.

Step 4. Pick up new constants $\lambda_2, \ldots, \lambda_M$ and go to Step 1 until the solution manifolds are numerically traced.

Step 5. Pick up some specific points on the solution manifold and compute $\Phi_j(x,t) = \mathrm{e}^{-\mathbf{i}\lambda_j t} u_j(x)$ for various values of the time variable t.

Remark 4.2. If Algorithm 4.1 is executed on a sequential computer, then we only can pick up a new constant, say, λ_2, and fix the remaining parameters $\lambda_3, \ldots, \lambda_M$.

Remark 4.3. It is very flexible to choose some chemical potentials as the first continuation parameter. For instance, we may choose $\lambda_1 = \lambda_2$ or $\lambda_1 = \lambda_3$ or $\lambda_1 = \lambda_2 = \lambda_3$, and so forth.

We briefly address here that starting point used in Algorithm 4.1 is some point on the trivial solution curve which is close enough to the bifurcation point. Actually, any stationary state solution of Eq. (3) can be used as a starting point in the context of predictor–corrector continuation methods. All we need to do is to make a change of variable using the given initial data. This will switch the starting point to some point on the trivial solution curve again. See e.g. [22] for details. In Algorithm 4.1 probably we cannot use any general function as the initial data in the state space, it is very flexible to choose parameters as the initial data in the parameter space.

4.2. Mass conservation constraints

If we impose the mass conservation constraints Eq. (8) on Eq. (4), it would be easier to implement Algorithm 4.1 for computing wave functions of the MCNLS, since we only need to obtain at almost M points on the solution manifolds that satisfy $\|u_j(x)\|_2 = 1$ for different values of $\lambda_{1,j}$, $j = 1, \ldots, M$. On the other hand, we can choose a relatively large stepsize so that the target points can be reached as soon as possible, because the other parts of the solution curves can be roughly approximated.

Remark 4.4. (i) In implementing Algorithm 4.1, it is quite impossible that we will hit, e.g., the jth component $u_j(x)$ with $\|u_j^{(k)}(x)\|_2 = 1$ precisely, say at the kth continuation step. This problem can be easily overcome by using the linear interpolation technique on the values of $(u_j^{(k)}(x), \lambda_{1,j}^{(k)})$ and $(u_j^{(k+1)}(x), \lambda_{1,j}^{(k+1)})$ with $\|u_j^{(k)}(x)\|_2 < 1$ and $\|u_j^{(k+1)}(x)\|_2 > 1$, where a small stepsize should be used when we approach the target point. (ii) In practice,

we will touch certain target points $(u_j(x),\lambda_{1,j})$ with $\|u_j(x)\|_2 = 1$ for different values of $\lambda_{1,j}$. It is easy to modify Algorithm 4.1 so that (i) is satisfied.

5. Numerical results

We discretized the MCNLS defined on the unit disk by using the centered difference approximations with uniform mesh sizes $\Delta r = \frac{2}{201} \approx \frac{1}{100}$ and $\Delta\theta = \frac{2\pi}{72} \approx 0.087$. We treated λ_1 as the first continuation parameter in our continuation algorithm, where Gaussian elimination and the Bi-CGSTAB were used as the linear solver. We are mainly interested in the ground-state and the first excited-state solutions of the system.

Example 1. $M = 1$. Case (i): Nondegenerate and degenerate energies. We consider following equation

$$\begin{aligned} &-\left(\frac{\partial^2 u}{\partial r^2} + \frac{1}{r}\frac{\partial u}{\partial r} + \frac{1}{r^2}\frac{\partial^2 u}{\partial \theta^2}\right) - \lambda u + \mu u^3 = 0, \\ &u(1,\theta) = 0. \end{aligned} \tag{49}$$

Fig. 1 shows that the first bifurcation $(0,\lambda_{0,1})$ of Eq. (49) is supercritical or subcritical, depending on the coefficient $\mu > 0$ or $\mu < 0$. Fig. 2 depicts the two solution curves of Eq. (49) branching from the second bifurcation $(0,\lambda_{1,1})$, which shows that the two degenerate excited-states have the same energy. We stopped curve-tracking whenever the target points were obtained. Fig. 3 shows the nodal lines of the solution curves corresponding to $\cos\theta$ and $\sin\theta$ in Eq. (15) are located at $\theta = \frac{\pi}{2}$ and $\theta = 0$, and those corresponding to the basis in Eq. (16) are located at $\theta = \frac{\pi}{4}$ and $\theta = \frac{3\pi}{4}$, respectively.

Case (ii): The ground-state and excited-state solutions with the effect of linear potential and strong repulsive interaction. We consider a single NLS

$$\begin{aligned} &-\frac{\varepsilon^2}{2}\left(\frac{\partial^2 u}{\partial r^2} + \frac{1}{r}\frac{\partial u}{\partial r} + \frac{1}{r^2}\frac{\partial^2 u}{\partial \theta^2}\right) - \lambda u + Vu + \mu u^3 = 0 \quad \text{in } \Omega, \\ &u(1,\theta) = 0, \quad 0 \leqslant \theta < 2\pi \end{aligned} \tag{50}$$

with $\varepsilon = 0.1$, $\mu = 30$, and $V(x_1,x_2) = \frac{x_1^2+x_2^2}{2}$. Fig. 4 displays the four solution curves of Eq. (50) branching from the second bifurcation point $(0,\lambda_{1,1}) \approx (0, 0.200656)$. The corresponding contours are shown in Fig. 5.

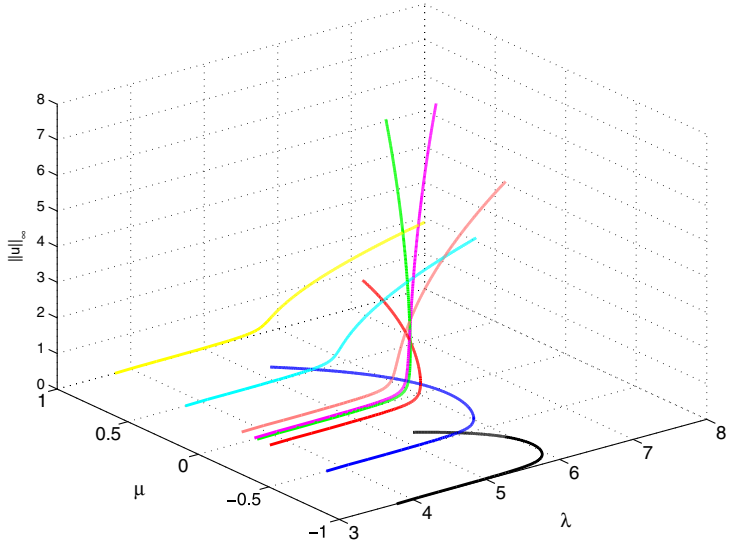

Fig. 1. The solution surface of Eq. (49) with $\mu \in [-1,1]$.

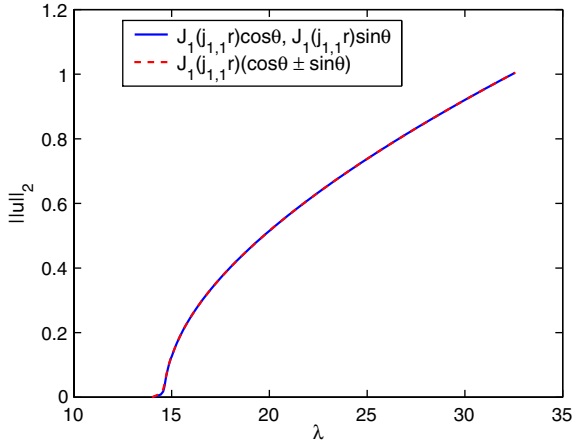

Fig. 2. The solution curves of Eq. (49) with $\mu = 30$ branching from $(0, \lambda_{1,1})$.

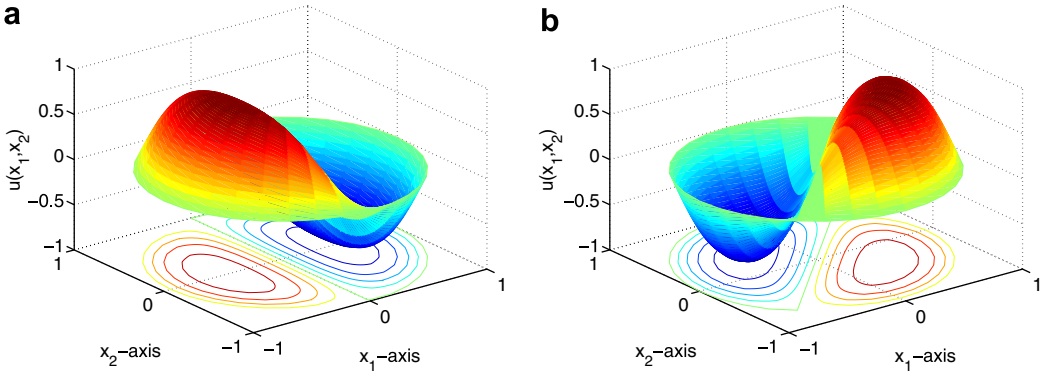

Fig. 3. The contours of the solution curves of Eq. (49) with $\mu = 30$ bifurcating at $(0, \lambda_{1,1})$.

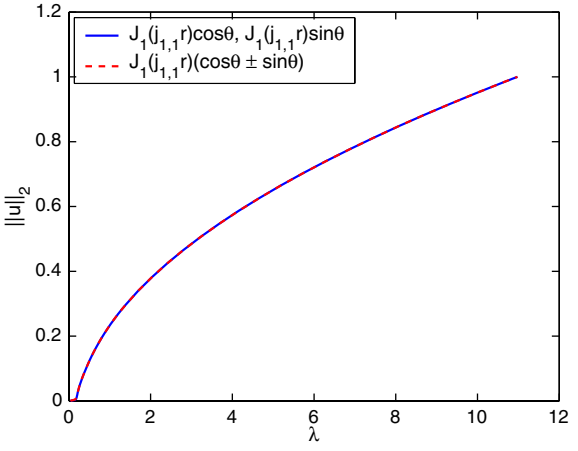

Fig. 4. The solution curves of Eq. (50) branching from the second bifurcation point, where $\varepsilon = 0.1$, $\mu = 30$, and $V(x_1, x_2) = \frac{x_1^2 + x_2^2}{2}$.

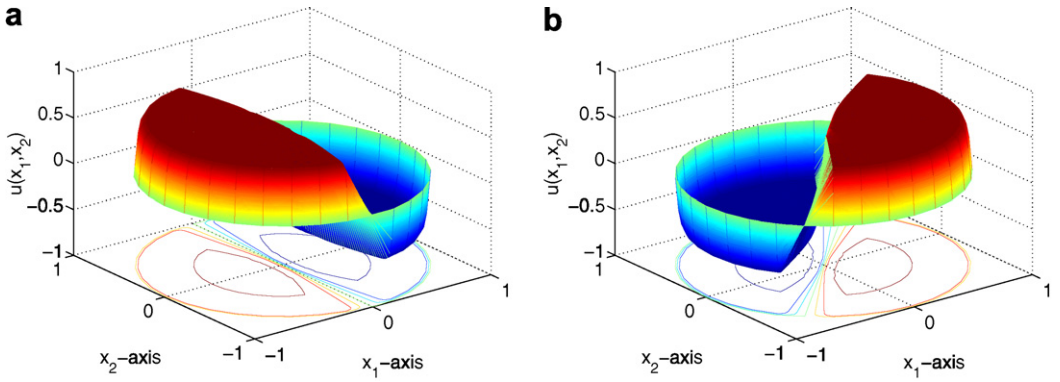

Fig. 5. The contours of the solution curves of Eq. (50) bifurcating at the second bifurcation point, where $\varepsilon = 0.1$, $\mu = 30$, and $V(x_1, x_2) = \frac{x_1^2 + x_2^2}{2}$.

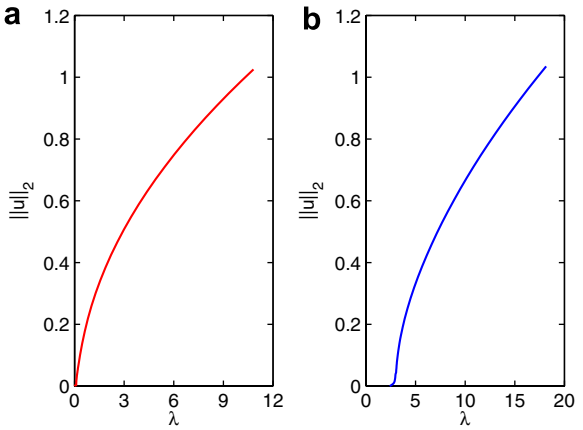

Fig. 6. The solution curves of Eq. (50) branching from the first bifurcation point, where $\varepsilon = 0.1$ (left), and $\varepsilon = 1.0$ (right).

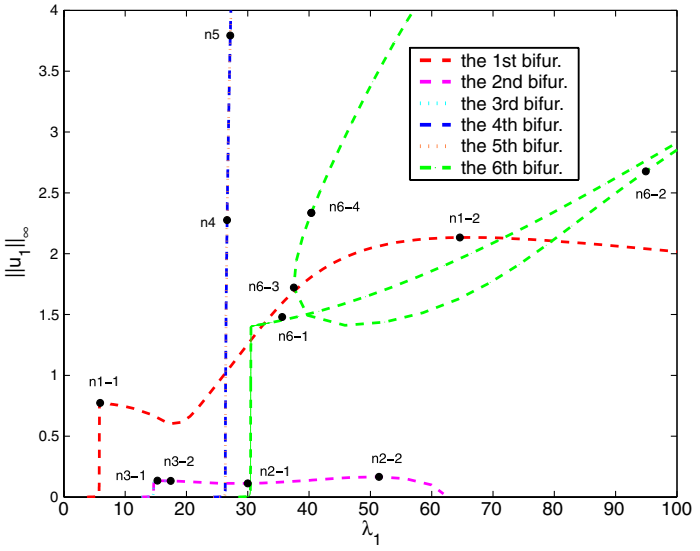

Fig. 7. The solution curves of the u_1-component branching from the first six bifurcations of Eq. (40) at $\lambda_2 = 15.0$, $\beta = 30.0$, $\mu_1 = \mu_2 = 0.1$.

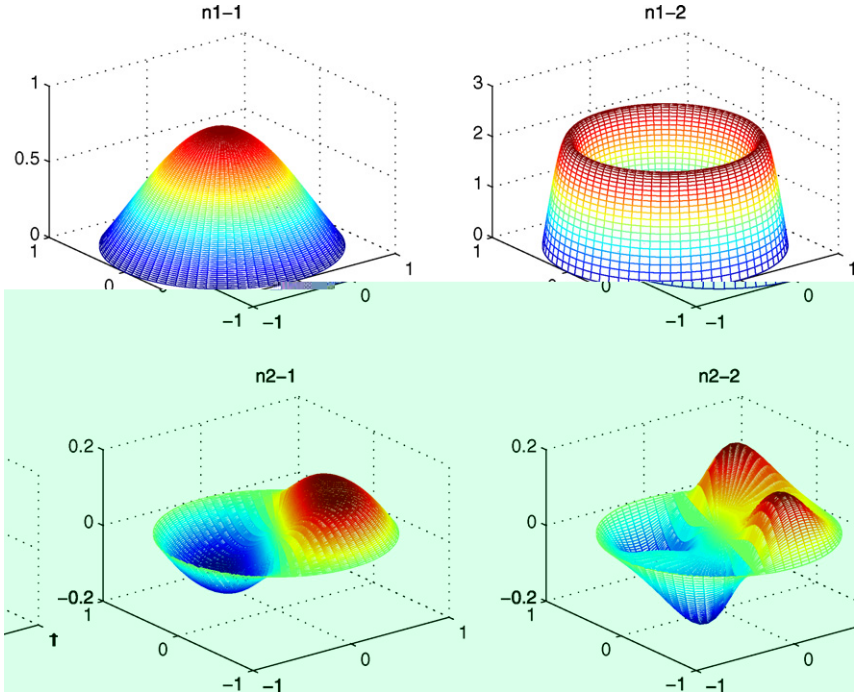

Fig. 8. The contours of the solutions of u_1-component for Eq. (40) at the nodes n1-1, n1-2, n2-1 and n2-2.

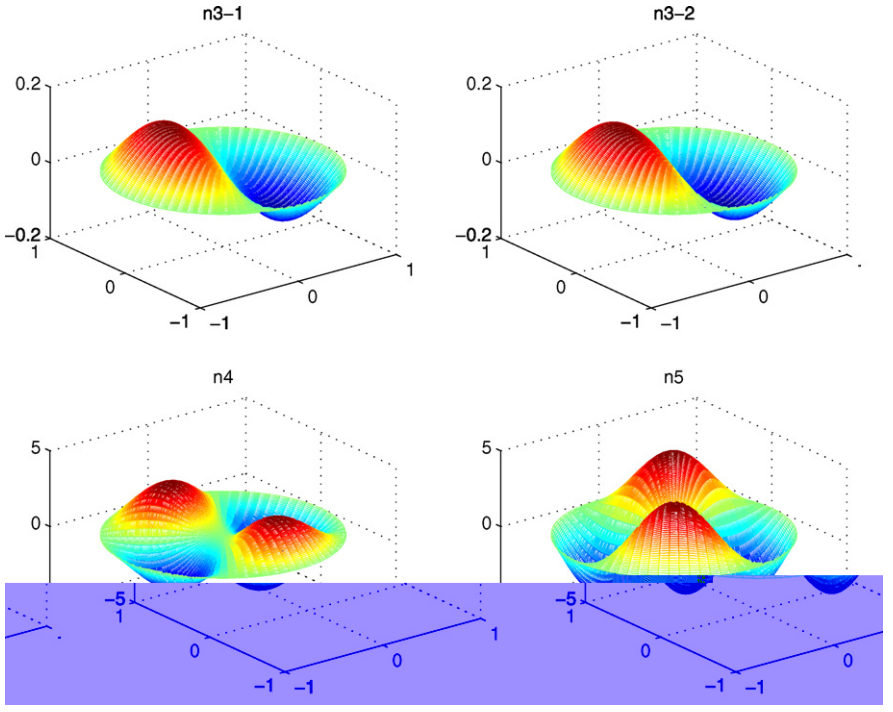

Fig. 9. The contours of the u_1-component on the solution branches of Eq. (40) at nodes n3-1, n3-2, n4 and n5.

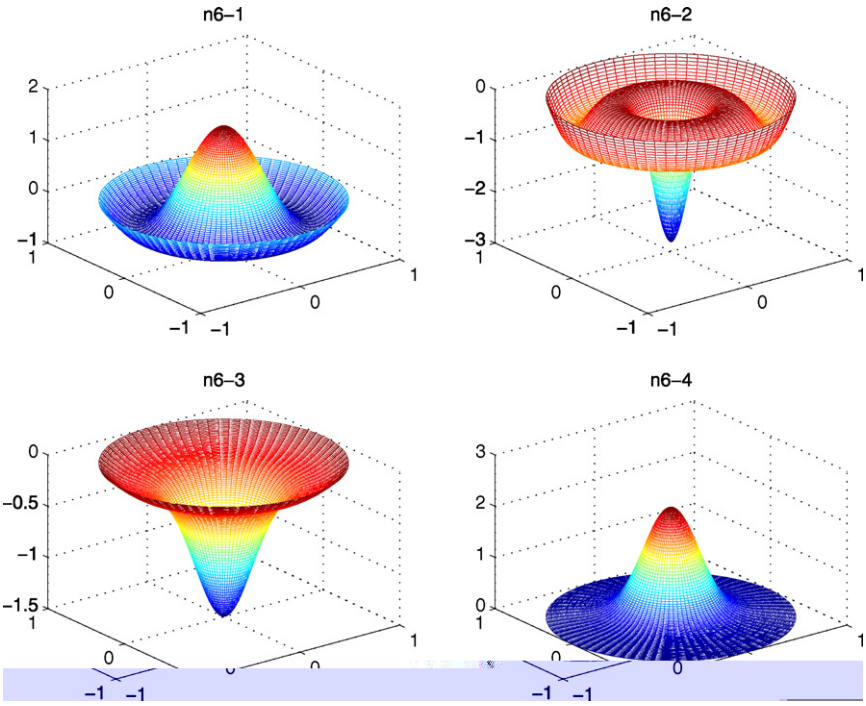

Fig. 10. The contours of the u_1-component on the six solution branch of Eq. (40) at nodes n6-1, n6-2, n6-3 and n6-4.

Case (iii): The ground-state solution with the effect of strong and weak repulsive interactions. We consider Eq. (50) with $\mu = 30$ and $V(x_1, x_2) = \frac{x_1^2+x_2^2}{2}$. For the strong and weak repulsive interactions, we chose $\varepsilon = 0.1$ and $\varepsilon = 1$, respectively. Fig. 6 displays the solution curves branching from the first bifurcation point for both cases, where the bifurcation points are detected at $(0,\lambda_{0,1}) \approx (0, 0.100068)$ and $(0, 2.999835)$, respectively. Fig. 6a shows that the ground-state energy of a quantum particle with strong repulsive interaction is less than that with weak repulsive interaction.

From cases (ii) and (iii) we observe that the first two bifurcations of the system are getting closer if the interaction is strongly repulsive.

Example 2. $M = 2$. The ground-state and excited-state solutions with the effect of isotropic and nonisotropic linear potentials. First, we consider Eq. (40) without linear potentials, where we chose $\lambda_2 = 15.0$, $\mu_1 = \mu_2 = 0.1$, and treated λ_1 as the continuation parameter with $\beta \in [-3000, 3000]$. Fig. 7 displays the solution curves of u_1 branching from the first six bifurcation points, where $\lambda_2 = 15.0$, $\beta = 30.0$, and $\mu_1 = \mu_2 = 0.1$. We observe that the second and the third bifurcations are double. Figs. 8–10 show the contours of the u_1-component at the nodes in Fig. 7. The contours of the u_1- and u_2-components on the sixth solution branch at $\lambda_1 = 30.4174$, -9.1226, -1100.2352, and -3851.9162 are displayed in Fig. 11, where $\lambda_2 = 30.0$, $\beta = -30.0$, and $\mu_1 = \mu_2 = 20.0$.

Next, we consider Eq. (40) with $V_1(x) = \frac{a_{11}x_1^2+a_{12}x_2^2}{2}$, $V_2(x) = \frac{a_{21}x_1^2+a_{22}x_2^2}{2}$ and $\lambda_2 = 15.0$, $\beta = -30.0$, $\mu_1 = \mu_2 = 0.1$. Fig. 12 shows the solution curves of the u_1-component branching from the first bifurcation point for various choices of linear potentials. Fig. 13 shows the contours of the u_1-component at $\lambda_1 = 6.0848$, 4.0930, -5.7564 and -149.6360, where we chose isotropic linear potentials with $a_{11} = a_{12} = 3$ and $a_{21} = a_{22} = 5$. Fig. 14 displays the wave functions Φ_1 and Φ_2 at $\lambda_1 = -149.6360$, $\lambda_2 = 15.0$ and $t = 0.1$, 0.2, 0.3, and 0.4. Fig. 15 shows the contours of the u_1-component at $\lambda_1 = 5.8589$, -30.2306, -306.3890, and -805.1825, respectively, where $V_1(x)$ is isotropic and $V_2(x)$ is nonisotropic with $a_{11} = a_{12} = 1$ and $a_{21} = 7$, $a_{22} = 1$, respectively.

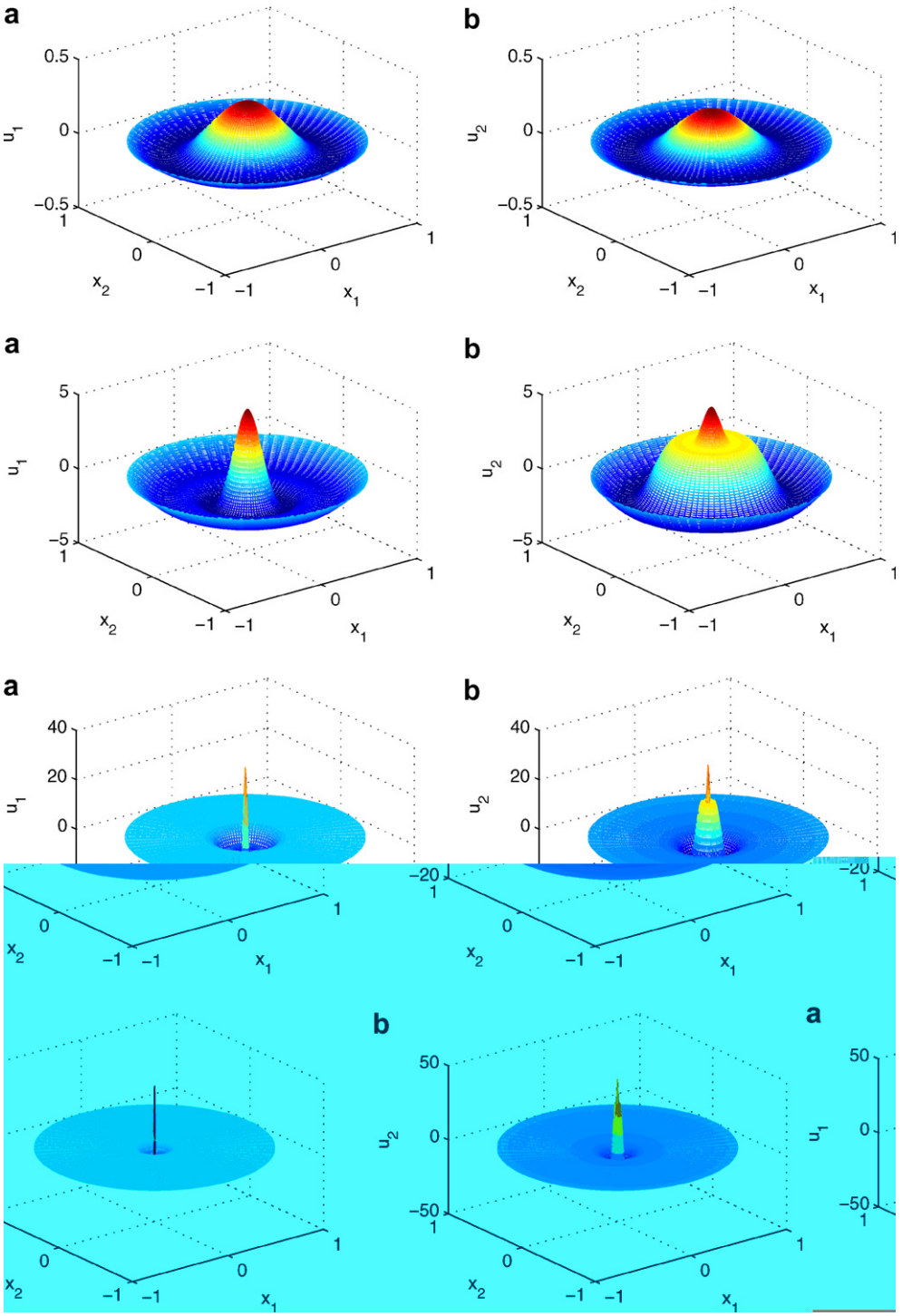

Fig. 11. The contours of the u_1- and u_2-components on the sixth solution branch of Eq. (40) at $\lambda_1 = 30.4174$, -9.1226, -1100.2352, -3851.9162.

Example 3. $M = 2$. The ground-state solution with the effect of isotropic linear potentials. We traced the first solution branch of Eq. (40) under the normalization conditions Eq. (8) with $V_1 = \frac{x_1^2+x_2^2}{2}$, $V_2 = \frac{x_1^2+x_2^2}{5}$, $\mu_1 = 10$, $\mu_2 = 5$, $\lambda_2 = 10$. Fig. 16 shows that both components can reach $\|u_j(x)\|_2 = 1$, $j = 1,2$, with $\beta = -300$ for different values of the chemical potentials λ_1. The contours of the corresponding wave function Φ_1 with $\|\Phi_1\|_2 = 1$ at $t = 0.5$ and 1 are displayed in Fig. 17. Fig. 18 shows that only the component u_2 satisfies the normalization conditions equation (8) where $\beta = 300$. Fig. 19 shows the contours of the wave function Φ_2 with $\|\Phi_2\|_2 = 1$ at $t = 13$ and 17.

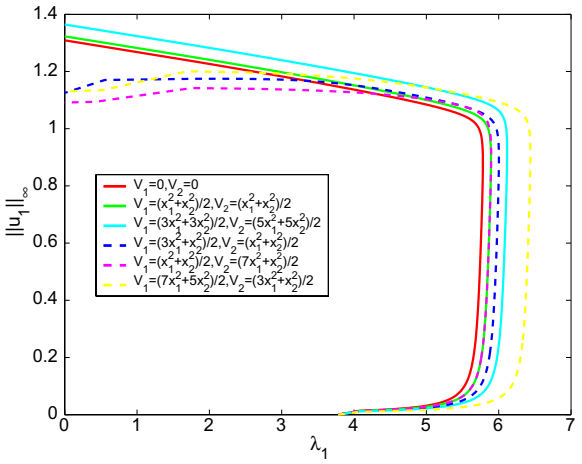

Fig. 12. The solution curves of the u_1-component branching from the first bifurcation point of Eq. (40).

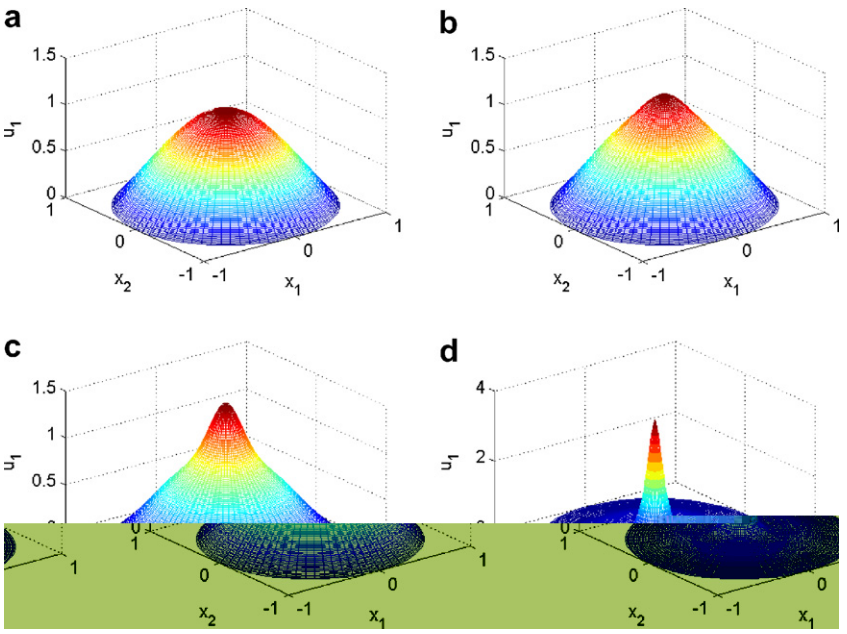

Fig. 13. The contours of the u_1-component on the first solution branch of Eq. (40) at $\lambda_1 = 6.0848$, 4.0930, -5.7564, -149.6360, respectively, where $V_1(x) = \frac{3x_1^2+3x_2^2}{2}$, $V_2(x) = \frac{5x_1^2+5x_2^2}{2}$.

Example 4. $M = 3$. The ground-state solution with the effect of isotropic and nonisotropic linear potentials. We traced the solution curves of the three-coupled NLS

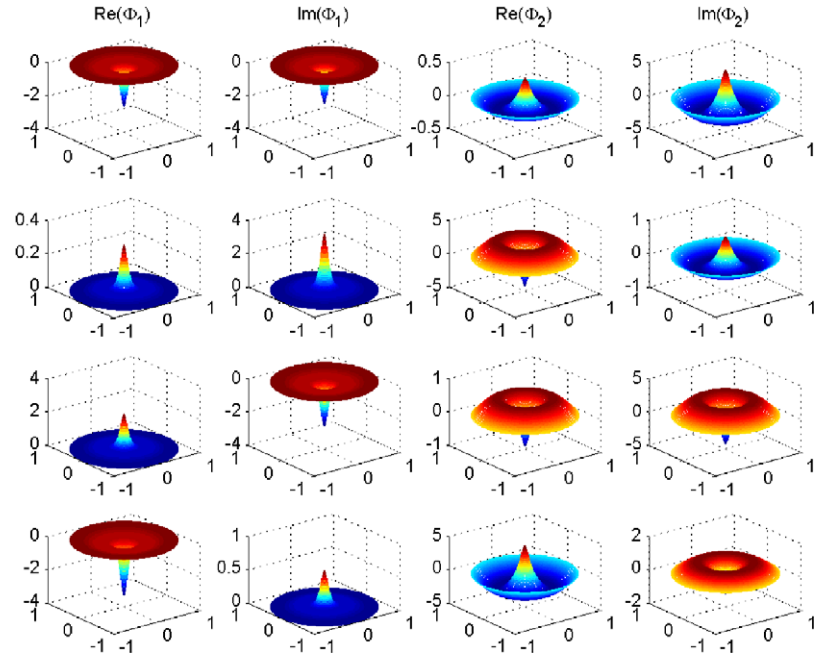

Fig. 14. The contours of the real and imaginary parts of the wave solutions $\Phi_j, j = 1,2$ at $\lambda_1 = -149.6360$, $\lambda_2 = 15.0$ and $t = 0.1$, 0.2, 0.3, and 0.4.

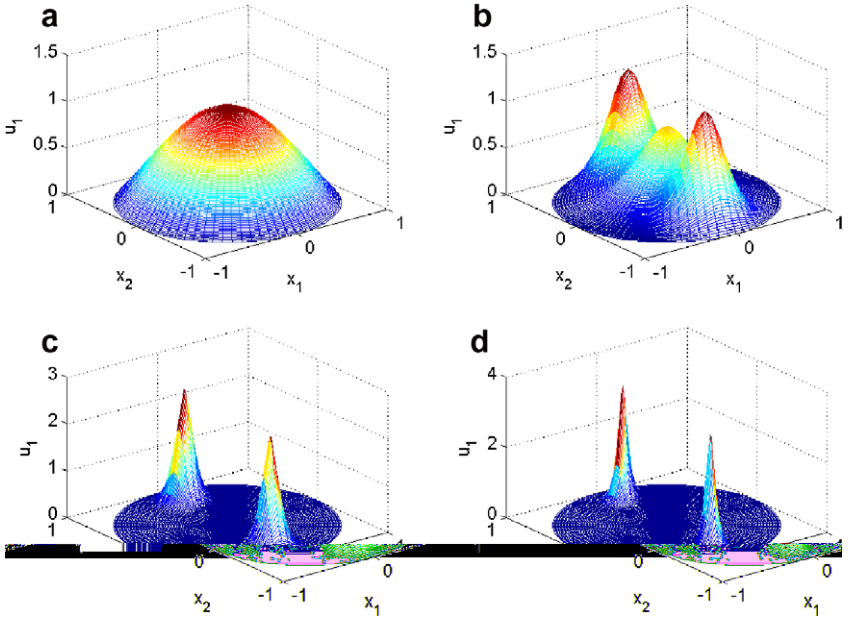

Fig. 15. The contours of the solutions of Eq. (40) for u_1 at $\lambda_1 = 5.8589$, -30.2306, -306.3890, -805.1825, respectively, where $V_1(x) = \frac{x_1^2+x_2^2}{2}$, $V_2(x) = \frac{7x_1^2+x_2^2}{2}$.

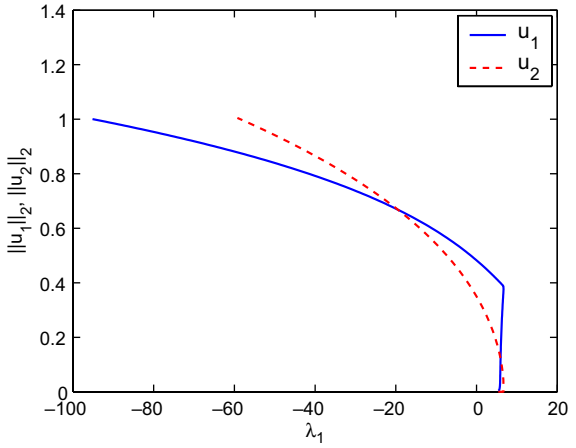

Fig. 16. Tracing the solution curves of Eq. (40) branching from the first bifurcation point until $\|u_1\|_2 = 1$ and $\|u_2\|_2 = 1$ are reached, where $\beta = -300$.

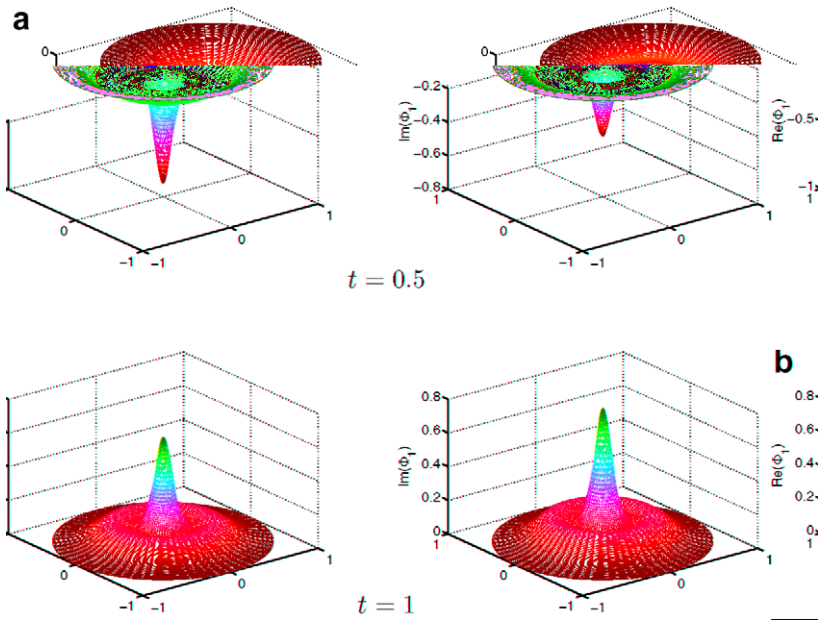

Fig. 17. The contours of the real and imaginary parts of the wave solutions Φ_1 with $\lambda_1 = -95.15455$ and $\|\Phi_1\|_2 = 1$ at $t = 0.5$, 1, and $\beta = -300$.

$$
\begin{aligned}
&-\left(\frac{\partial^2 u_1}{\partial r^2}+\frac{1}{r}\frac{\partial u_1}{\partial r}+\frac{1}{r^2}\frac{\partial^2 u_1}{\partial \theta^2}\right)-\lambda_1 u_1+V_1(r,\theta)u_1+\mu_1 u_1^3+\beta_{12}u_2^2u_1+\beta_{13}u_3^2u_1=0,\\
&-\left(\frac{\partial^2 u_2}{\partial r^2}+\frac{1}{r}\frac{\partial u_2}{\partial r}+\frac{1}{r^2}\frac{\partial^2 u_2}{\partial \theta^2}\right)-\lambda_2 u_2+V_2(r,\theta)u_2+\mu_2 u_2^3+\beta_{12}u_1^2u_2+\beta_{23}u_3^2u_2=0, \quad \text{in } \Omega,\\
&-\left(\frac{\partial^2 u_3}{\partial r^2}+\frac{1}{r}\frac{\partial u_3}{\partial r}+\frac{1}{r^2}\frac{\partial^2 u_3}{\partial \theta^2}\right)-\lambda_3 u_3+V_3(r,\theta)u_3+\mu_3 u_3^3+\beta_{13}u_1^2u_3+\beta_{23}u_2^2u_3=0,\\
&u_1(1,\theta)=u_2(1,\theta)=u_3(1,\theta)=0, \quad 0\leqslant\theta\leqslant 2\pi,
\end{aligned}
\tag{51}
$$

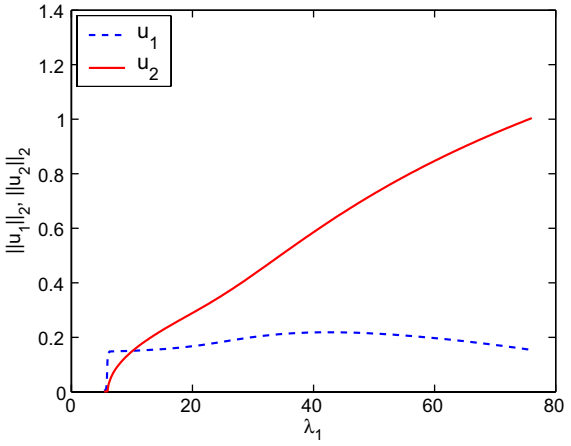

Fig. 18. Tracing the solution curves of Eq. (40) branching from the first bifurcation point until $\|u_2\|_2 = 1$ is reached, where $\beta = 300$.

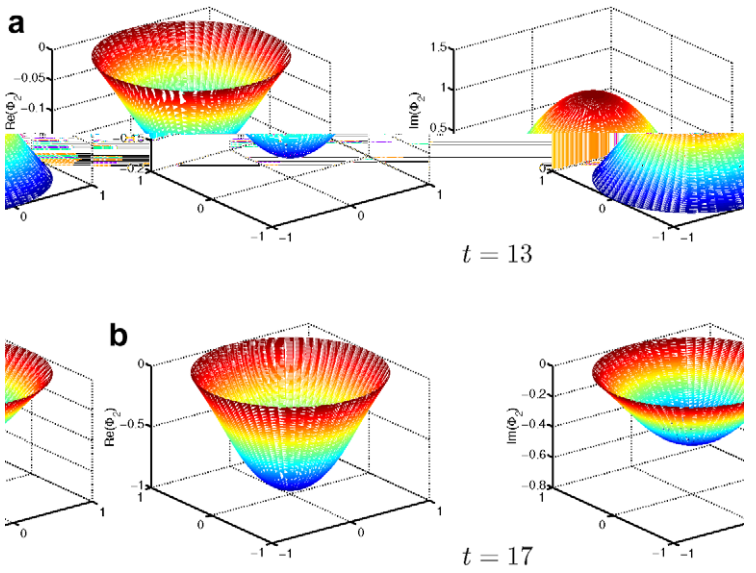

Fig. 19. The contours of the real and imaginary parts of the wave solutions Φ_2 with $\lambda_1 = 76.0517664$ and $\|\Phi_2\|_2 = 1$ at $t = 13$, 17, and $\beta = 300$.

where $\lambda_2 = 15.0$, $\lambda_3 = 20.0$, $\mu_1 = \mu_2 = \mu_3 = 0.1$, $\beta_{12} = 30.0$, $\beta_{13} = 60.0$, $\beta_{23} = 90.0$, and $V_1(x) = \frac{3x_1^2+x_2^2}{2}$, $V_2(x) = \frac{5x_1^2+x_2^2}{2}$, $V_3(x) = \frac{7x_1^2+x_2^2}{2}$. Fig. 20 depicts the solution curves of (u_1, u_2, u_3) branching from the first bifurcation point of Eq. (51). The contours of the real and imaginary parts of the wave solutions Φ_j, $j = 1, 2, 3$ at $(\lambda_1, \lambda_2, \lambda_3) = (17.0271, 15.0, 20.0)$, and $t = 1000$ are displayed in Fig. 21. We also chose $\lambda_2 = 15.0$, $\lambda_3 = 20.0$, $\mu_1 = \mu_2 = \mu_3 = 0.1$, $\beta_{12} = -30.0$, $\beta_{13} = -60.0$, $\beta_{23} = -90.0$ and $V_1(x) = V_2(x) = V_3(x) = \frac{x_1^2+x_2^2}{2}$. Fig. 22 shows that the solution curves of (u_1, u_2, u_3) have a fold at $\lambda_1 = -7.110808$. Figs. 20 and 22 show that all three components $u_j(x)$ satisfy $\|u_j(x)\|_2 = 1$ for different values of chemical potentials.

6. Conclusions

We have presented a novel algorithm for computing wave functions of the MCNLS. We indicate that the wave functions can be obtained by solving the stationary state of the MCNLS, which is a nonlinear system of

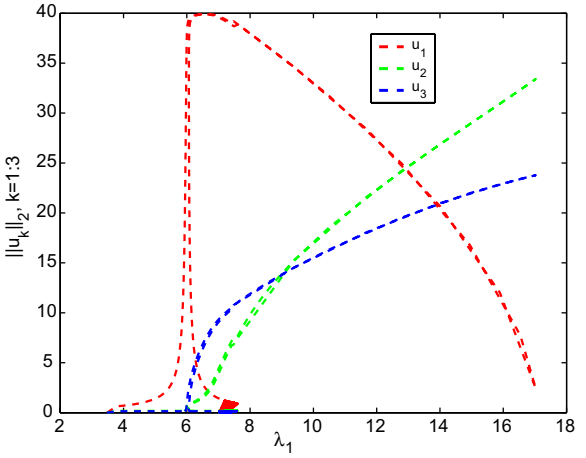

Fig. 20. The solution curves (u_1,u_2,u_3) branching from the first bifurcation point of Eq. (51) at $\lambda_2 = 15.0$, $\lambda_3 = 20.0$, $\mu_1 = \mu_2 = \mu_3 = 0.1$, $\beta_{12} = 30.0$, $\beta_{13} = 60.0$, $\beta_{23} = 90.0$ and $V_1(x) = \frac{3x_1^2+x_2^2}{2}$, $V_2(x) = \frac{5x_1^2+x_2^2}{2}$, $V_3(x) = \frac{7x_1^2+x_2^2}{2}$.

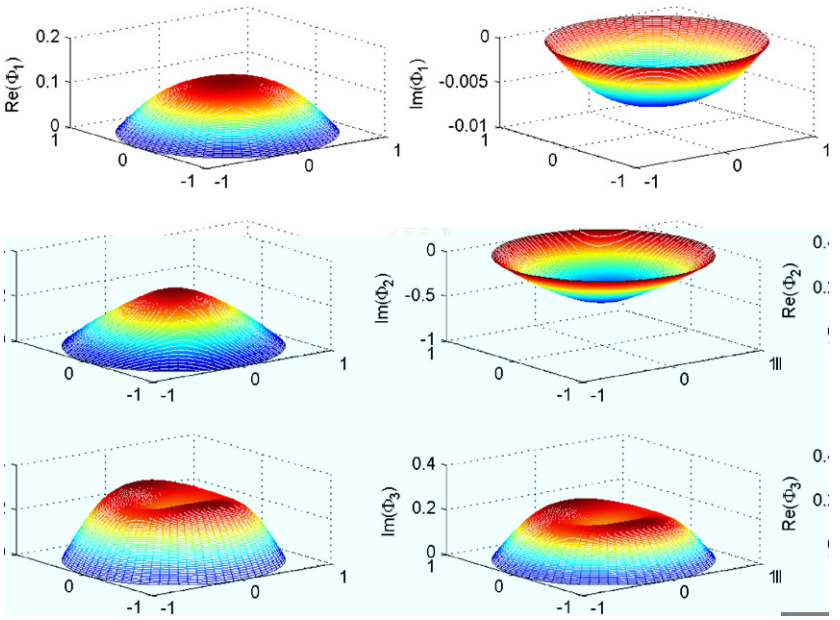

Fig. 21. The contours of the real and imaginary parts of the wave solutions Φ_j, $j = 1,2,3$ with $\lambda_1 = 17.0271$, $\lambda_2 = 15.0$, $\lambda_3 = 20.0$, respectively, at $t = 1000$.

equations. We exploited a parallel numerical continuation algorithm proposed in [19] to trace solution manifolds of the nonlinear system. It is inexpensive to implement the algorithm because in practice we only need to compute some specific points on the solution manifolds whenever a solution curve is numerically traced. The proposed algorithm has the following advantages: (i). It is unnecessary to discretize or integrate $\frac{\partial}{\partial t}\Phi_j(x,t)$, $j = 1,\ldots,M$. (ii). The wave functions $\Phi_j(x,t)$ can be evaluated for any time scale t, and for any points $\{(u_j,\lambda_j)\}_{j=1:M}$ on the solution manifolds. (iii). The mass conservation constraints are a benefit to numerical continuation methods.

Next, we have analyzed the relationship among the energy levels of a quantum particle, the associated eigenvalues of the SEP, and the corresponding bifurcations of the NLS. We have shown that the energy level

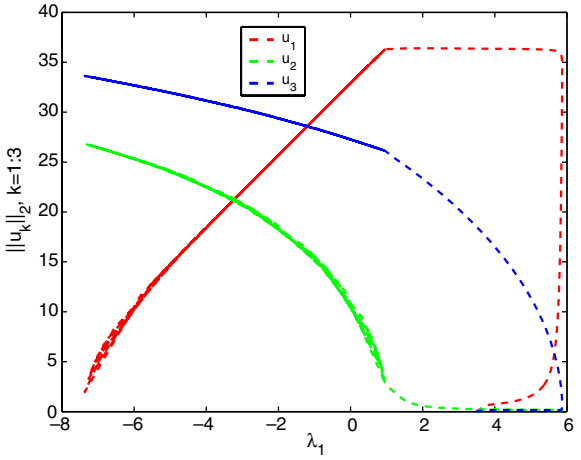

Fig. 22. The solution curves (u_1, u_2, u_3) of Eq. (51) at $\lambda_2 = 15.0$, $\lambda_3 = 20.0$, $\mu_1 = \mu_2 = \mu_3 = 0.1$, $\beta_{12} = -30.0$, $\beta_{13} = -60.0$, $\beta_{23} = -90.0$ and $V_1(x) = V_2(x) = V_3(x) = \frac{x_1^2 + x_2^2}{2}$.

of the SEP can be used as an initial guess to computing their counterpart of the NLS, where the continuation method is used as the iterative scheme. Based on the numerical results reported in Section 5, we wish to given some conclusions concerning the performance of the proposed algorithm and the physical meaning of the results. (a) When the NLS has strong repulsive interaction, the first bifurcation point is close to origin. See Figs. 4 and 6. Actually, if $\varepsilon \to 0$, then the first bifurcation will be very close to the origin, which means that less chemical potential is required for the occurrence of the first bifurcation. On the other hand, more chemical potential is necessary if the system has weak repulsive interaction. (b) For the two-coupled NLS, both components satisfy the mass conservation constraint if the coupling coefficient β is greater than zero, otherwise only the second component satisfies the mass conservation constraint. (c) The results of Example 2 show that the global bifurcation behavior of the two-coupled NLS varies with respect to the locations of the bifurcations.

Finally, we remark here that the $u_j(x)$ in Eq. (2) are real functions. In a rotating BEC where the angular momentum is imposed on the system, the stationary state functions $u_j(x)$ must be complex, see e.g. [4,23]. It would be of interest to study the bifurcation behavior of the MCNLS with angular momentum defined in a cylindrical domain. The details will be given elsewhere.

Acknowledgment

Supported by the National Science Council of ROC (Taiwan) through Project NSC 95-2115-M-005-004-MY3.

References

[1] M. Abramowitz, I.A. Stegun, Handbook of Mathematical Functions, National Bureau of Standards, Washington, DC, 1964.
[2] S.K. Adhikari, Numerical study of the spherically symmetric Gross–Pitaevskii equation in two space dimensions, Phys. Rev. E 62 (2000) 2937–2944.
[3] S.K. Adhikari, P. Muruganandam, Bose–Einstein condensation dynamics from the numerical solution of the Gross–Pitaevskii equation, J. Phys. B 35 (2002) 2831–2843.
[4] A. Aftalion, Q. Du, Vortices in a rotating Bose–Einstein condensate: critical angular velocities and energy diagrams in the Thomas–Fermi regime, Phys. Rev. A 64 (2001) 063603.
[5] G.P. Agrawal, Nonlinear Fiber Optics, third ed., Academic Press, New York, 2001.
[6] N. Akhmediev, A. Ankiewice, Partially coherent solitons on a finite background, Phys. Rev. Lett. 82 (1999) 2661–2664.
[7] E.L. Allgower, K. Georg, Introduction to Numerical Continuation Methods, SIAM Publications, Philadelphia, 2003.
[8] M.H. Anderson, J.R. Ensher, M.R. Matthews, C.E. Wieman, E.A. Cornell, Observation of Bose–Einstein condensation in a dilute atomic vapor, Science 269 (1995) 198–201.

[9] J.R. Anglin, W. Ketterle, Bose–Einstein condensation of atomic gases, Nature 416 (2002) 211–218.
[10] R.E. Bank, T.F. Chan, PLTMGC: a multi-grid continuation program for parameterized nonlinear elliptic systems, SIAM J. Sci. Stat. Comput. 7 (1986) 540–559.
[11] W. Bao, Q. Du, Computing the ground state solution of Bose–Einstein condensates by a normalized gradient flow, SIAM J. Sci. Comput. 25 (2004) 1674–1697.
[12] W. Bao, D. Jaksch, P.A. Markowich, Numerical solution of the Gross–Pitaevskii equation for Bose–Einstein condensation, J. Comput. Phys. 187 (2003) 318–342.
[13] W. Bao, S. Jin, P.A. Markowich, On time splitting spectral approximations for the Schrödinger equation in the semiclassical regime, J. Comput. Phys. 175 (2002) 487–524.
[14] W. Bao, S. Jin, P.A. Markowich, Numerical study of time-splitting spectral discretizations of nonlinear Schrödinger equations in the semiclassical regimes, SIAM J. Sci. Comput. 25 (2003) 27–64.
[15] W. Bao, W. Tang, Ground-state solution of Bose–Einstein condensate by directly minimizing the energy functional, J. Comput. Phys. 187 (2003) 230–254.
[16] K. Böhmer, Z. Mei, Mode interactions of an elliptic system on the square, International Series on Numerica Mathematics, vol. 104, Birkhäuser, Basel, 1992, pp. 49–58.
[17] C.C. Bradley, C.A. Sackett, R.G. Hulet, Bose–Einstein condensation of lithium: observation of limited condensate number, Phys. Rev. Lett. 78 (1997) 985–989.
[18] S.-L. Chang, C.-S. Chien, Numerical continuation for nonlinear Schrödinger equations, Int. J. Bifurc. Chaos (to appear).
[19] S.-L. Chang, C.-S. Chien, B.-W. Jeng, Tracing the solution surface with folds of a two-parameter system, Int. J. Bifurc. Chaos 15 (2005) 2689–2700.
[20] S.-L. Chang, C.-S. Chien, B.-W. Jeng, Liapunov–Schmidt reduction and continuation for nonlinear Schrödinger equations, SIAM J. Sci. Comput. 29 (2007) 729–755.
[21] C.-S. Chien, B.-W. Jeng, A two-grid discretization scheme for semilinear elliptic eigenvalue problems, SIAM J. Sci. Comput. 27 (2006) 1287–1304.
[22] C.-S. Chien, Z. Mei, C.-L. Shen, Numerical continuation at double bifurcation points of a reaction-diffusion problem, Int. J. Bifurc. Chaos 8 (1998) 117–139.
[23] S.A. Chin, E. Krotscheck, Fourth-order algorithm for solving the imaginary-time Gross–Pitaevskii equation in a rotating anisotropic trap, Phys. Rev. E 72 (2005) 036705.
[24] M. Golubitsky, D.G. Schaeffer, Singularities and Groups in Bifurcation Theory, vol. I, Springer, New York, 1985.
[25] M. Gobulitsky, I. Stewart, D.G. Schaeffer, Singularities and Groups in Bifurcation Theory, vol. II, Springer, New York, 1988.
[26] D.S. Hall, M.R. Matthews, J.R. Ensher, C.E. Wieman, E.A. Cornell, Dynamics of component separation in a binary mixture of Bose–Einstein condensates, Phys. Rev. Lett. 81 (1998) 1539–1542.
[27] M. Haelterman, A. Sheppard, Bifurcation phenomena and multiple soliton-bound states in isotropic Kerr media, Phys. Rev. E 49 (1994) 3376–3381.
[28] R.A. Horn, C.R. Johnson, Matrix Analysis, Cambridge University Press, Cambridge, 1985.
[29] H.B. Keller, Lectures on Numerical Methods in Bifurcation Problems, Springer, Berlin, 1987.
[30] J.R. Kuttler, V.G. Sigillito, Eigenvalues of the Laplacian in two dimensions, SIAM Rev. 26 (1984) 163–193.
[31] M.-C. Lai, A note on finite difference discretizations for Poisson equation on a disk, Numer. Methods Partial Differential Eq. 17 (2001) 199–203.
[32] T.-C. Lin, J. Wei, Ground state of N coupled nonlinear Schrödinger equations in R^n, $n \leqslant 3$, Comm. Math. Phys. 255 (2005) 629–653.
[33] A. Minguzzi, S. Succi, F. Toschi, M.P. Tosi, P. Vignolo, Numerical methods for atomic quantum gases with applications to Bose–Einstein condensates and to ultracold fermions, Phys. Rep. 395 (2004) 223–355.
[34] P. Muruganandam, S.K. Adhikari, Bose–Einstein condensation dynamics in three dimensions by the pseudospectral and finite-difference methods, J. Phys. B 36 (2003) 2501–2513.
[35] L.P. Pitaevskii, Vortex lines in an imperfect Bose gas, Soviet Phys. JETP 13 (1961) 451–454.
[36] B.I. Schneider, D.L. Feder, Numerical approach to the ground and excited states of a Bose–Einstein condensed gas confined in a completely anisotropic trap, Phys. Rev. A 59 (1999) 2232–2242.
[37] J. Shen, Efficient spectral-Galerkin methods III: polar and cylindrical geometries, SIAM J. Sci. Comput. 18 (1997) 1583–1604.
[38] R.P. Tiwari, A. Shukla, A basis-set based Fortran program to solve the Gross–Pitaevskii equation for dilute Bose gases in harmonic and anharmonic traps, Comput. Phys. Commun. 174 (2006) 966–982.
[39] H.A. van der Vorst, Bi-CGSTAB: A fast and smoothly converging variant of Bi-CG for the solution of nonsymmetric linear systems, SIAM J. Sci. Stat. Comput. 13 (1992) 631–644.
[40] H.Q. Wang, Numerical studies on the split-step finite difference method for nonlinear Schrödinger equations, Appl. Math. Comput. 170 (2005) 17–35.